



ChemComm

**Step-Growth Polymerization by RAFT Process**

Journal:	<i>ChemComm</i>
Manuscript ID	CC-FEA-03-2023-001087.R2
Article Type:	Feature Article

SCHOLARONE™  
Manuscripts

## Step-Growth Polymerization by RAFT Process

Joji Tanaka,<sup>a\*</sup> Jiajia Li,<sup>a,b</sup> Samantha Maria Clouthier,<sup>a</sup> Wei You<sup>a\*</sup>

<sup>a</sup> Department of Chemistry, University of North Carolina, Chapel Hill, NC 27599, USA

<sup>b</sup> State and Local Joint Engineering Laboratory for Novel Functional Polymeric Materials, Jiangsu Key Laboratory of Advanced Functional Polymer Design and Application, Department of Polymer Science and Engineering, College of Chemistry, Chemical Engineering and Materials Science, Soochow University, Suzhou, China.

### Abstract

Reversible addition-Fragmentation Chain transfer (RAFT) step-growth polymerization is an emerging method that synergistically combines benefits of RAFT polymerization (functional group and user-friendly nature) and step-growth polymerization (versatility of the polymer backbone). This new polymerization method is generally achieved by using bifunctional reagents of monomer and Chain Transfer Agent (CTA) that efficiently yields Single monomer Unit Insertion (SUMI) adducts under stoichiometrically balanced conditions. This review covers a brief history of the RAFT-SUMI process and its transformation into RAFT step-growth polymerization, followed by a comprehensive discussion of various RAFT step-growth systems. Furthermore, characterizing the molecular weight evolution of step-growth polymerization is elaborated based on the Flory model. Lastly, a formula is introduced to describe the efficiency of RAFT-SUMI process, assuming rapid chain transfer equilibrium. Examples of reported RAFT step-growth and SUMI systems are then categorized based on the driving force.

## 1. Introduction

### 1.1 From RAFT chain-growth to RAFT step-growth

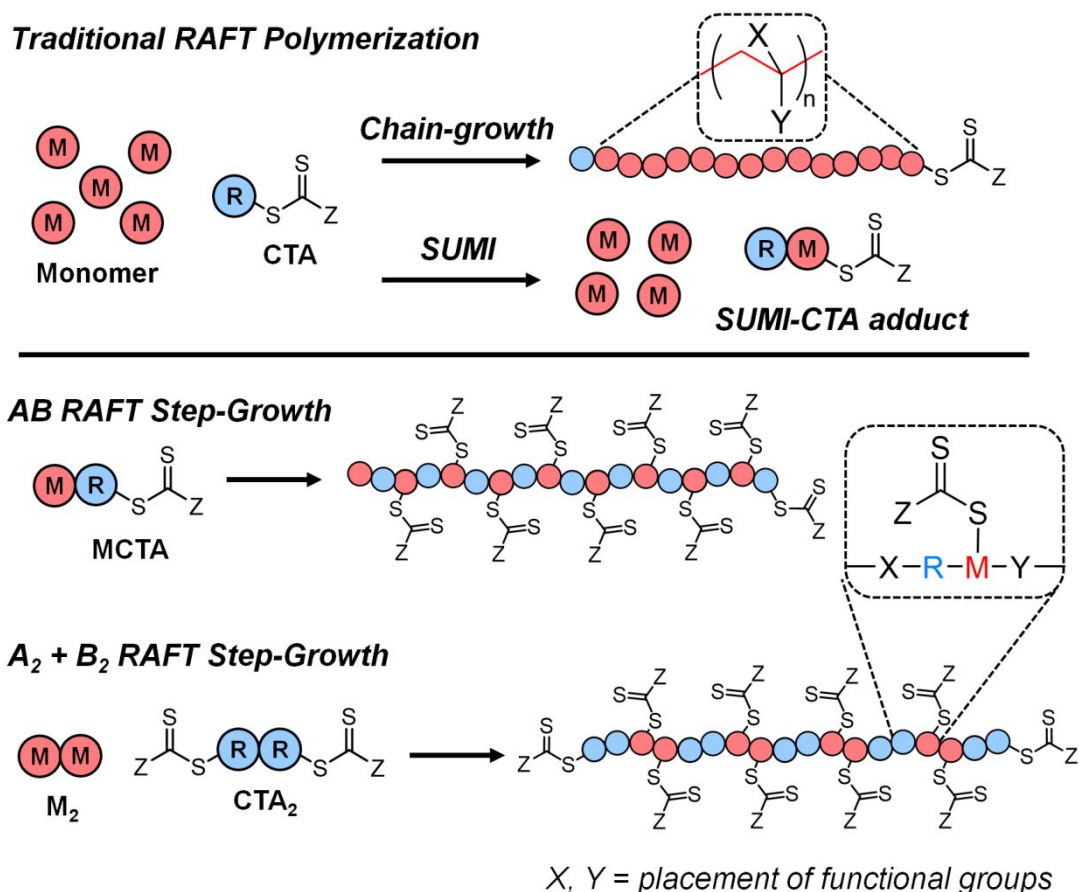
Polymer chemistry has been a growing field in synthetic chemistry with emergence of novel polymerization methods to design materials with unique features and properties.<sup>1-4</sup> Broadly speaking, most of these polymerization methodologies can be categorized into two common classes based on the polymerization mechanism and molecular weight evolution: step-growth and chain-growth. We note that there has been disputes on these terminologies and IUPAC recommended the use of polyaddition and chain polymerization, respectively.<sup>5</sup>

Chain-growth is a process where the polymers chains are seeded from an initiating source and the polymer chains grow by addition of the monomer to the chain end until the propagating end is terminated. Controlling this chain-growth process (e.g., living/controlled anionic/cationic/radical polymerization, ring-opening metathesis polymerization (ROMP), etc.) allows uniform growth of polymer chains, synthesis of block copolymers and complex polymer architectures, for a variety of applications.<sup>6</sup> The main drawback of chain-growth is the rather limited scope of the polymer backbone functionality, as the main chain is composed solely of the polymerized monomer units.

Step-growth on the other hand, grows by reacting two end groups together where all growing species have two reactive chain ends; however, compared to chain-growth, high conversion is required to gain appreciable molecular weight. Historically, this has been carried out via polycondensation, which typically requires harsh reaction conditions and is limited by low functional group tolerance.<sup>7</sup> Nevertheless, in contrast to chain growth, unique polymer backbones can be constructed for targeted applications as the functionalities can be placed independently between the two reacting sites – if such functionalities, built into the design of step-growth monomers, can remain intact under the polymerization condition.

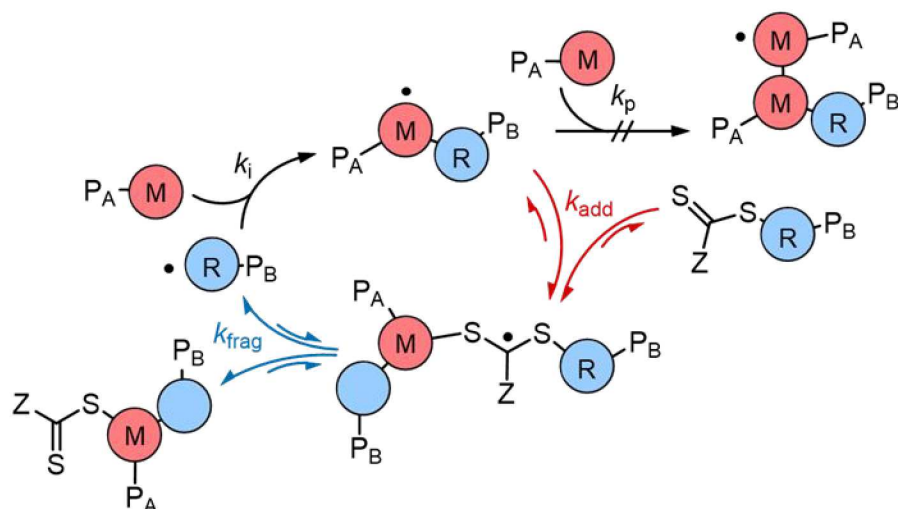
Free radical polymerization is a chain-growth process that has had implications in both academia and industry.<sup>8</sup> Many vinyl monomers can be polymerized through free radical polymerization without being hindered by common impurities.<sup>8</sup> Therefore, controlling this process through Reversible Deactivation Radical Polymerizations (RDRPs) methods has been a breakthrough since the late 20th century.<sup>9</sup> One of the leading platforms that has gained particular attention is Reversible-addition fragmentation Chain transfer (RAFT) polymerization.<sup>10</sup>

The RAFT process is mediated by thiocarbonylthio based Chain Transfer Agents (CTA) that seed chain-growth polymerization and govern the chain transfer exchange via an intermediate compound.<sup>11, 12</sup> Among all RDRP methods, RAFT polymerization is considered to be the most user-friendly and versatile, allowing control over a wide selection of monomer families by choosing the appropriate CTA.<sup>9, 13</sup> Furthermore, owing to the relatively high functional group tolerance of thiocarbonylthio group, RAFT polymerization has enabled engineering of well-defined polymers with a variety of functionalities placed on the side chains and end groups of the polymers. However, inherent to the chain-growth nature of RAFT polymerization, such polymers usually consist of inert carbon atoms (e.g., C-C single bond); this unfortunate fact has posed significant challenges to applications where degradable functionality is crucial such as tissue engineering and plastics recycling.<sup>14</sup> To address this challenge, we recently discovered RAFT step-growth polymerization (or SUMI polyaddition<sup>15</sup>) via the Single Monomer Unit Insertion (SUMI) process, using stoichiometrically equivalent bifunctional reagents of CTA and monomer functional groups (**Scheme 1**).<sup>16</sup>



**Scheme 1.** Illustration of chain-growth, SUMI and step-growth by RAFT process and placement of functional groups. Reproduced with permission from ref.<sup>16</sup> Copyright 2021, with permission from American Chemical Society.

This unique step-growth polymerization proceeds via the chain transfer cycle (**Scheme 2**), analogous to thio-ene step-growth<sup>17</sup> and closely related to metal catalyzed radical polyaddition.<sup>18-20</sup> In theory, RAFT step-growth polymerization would inherit key benefits from both RAFT (e.g., functional group tolerance and user-friendly nature) and step-growth (e.g., functional backbone) to allow a great versatility in the polymer chain design by incorporating desired chemical functionalities pre-embedded in the bifunctional reagents. Furthermore, the CTA is formed in situ at each repeat unit of the backbone after the RAFT step-growth polymerization, enabling further architectural control by a second polymerization step via RAFT chain-growth.



**Scheme 2.** RAFT step-growth mechanism. The RAFT step-growth mechanism proceeds through cycle of the radical addition ( $k_i$ ) between the two end group species: monomer and R•, forming the backbone radical, followed by chain transfer with the CTA end group through reversible addition ( $k_{add}$ ) and fragmentation ( $k_{frag}$ ) of the intermediate, to regenerate the R• species and yield the polymer backbone. Reproduced with permission from ref.<sup>21</sup> Copyright 2022, with permission from American Chemical Society.

## 1.2 Scope of the review

In this review, we highlight the recent developments of RAFT step-growth as a platform for facile synthesis of functional linear backbone and graft copolymers. We start with a brief discussion of the historical context of RAFT-SUMI process, though a more detailed review can be found elsewhere.<sup>15, 22</sup> We then revisit the characterization of step-growth molecular weight by conventional Size Exclusion Chromatography (SEC) analysis, which is applicable to other step-growth approaches. After going through details on a variety of RAFT step-growth systems, we summarize the mechanistic classification of the RAFT-SUMI/step-growth polymerization, with an aim to expand the monomer scope.

## 2 RAFT-SUMI Process

### 2.1 Historical context of RAFT-SUMI

The term RAFT-SUMI was first coined in 2011 by Moad;<sup>23</sup> however, the first example of RAFT-SUMI reaction can be dated back to 1988 when Zard and co-workers demonstrated the addition of xanthate to a number of vinyl compounds (e.g., vinyl acetate, *N*-methylmaleimide) for organic synthesis.<sup>24, 25</sup> Importantly, Zard recognized the radical nature enabled chain process, and the low steady state concentration of the intermediate radical species in the proposed reaction mechanism.<sup>24</sup> Such insight eventually led to the independent discovery of Macromolecular Design by Interchange of Xanthate (MADIX) controlled polymerization (identical process to RAFT polymerization) by Rhodia (now Solvay).<sup>26</sup>

As RAFT gained popularity since its emergence in 1998,<sup>10</sup> Klumperman and co-worker carefully studied the early kinetics of polymerization of styrene with a RAFT agent, cyanoisopropyl dithiobenzoate (AD in **Figure 1**) in 2004. They showed that in the initial stage of the polymerization, the as formed R• (cyanoisopropyl radical, A in **Figure 1**) almost exclusively added to one styrene unit, and formed the SUMI product (ASD in **Figure 1**), prior to the formation of higher order adducts (e.g., AS<sub>2</sub>D) (higher order adducts were possible in this case since the ratio of [M] vs [CTA] was ~5).<sup>27</sup> Almost simultaneously, Chen et al. applied the identical RAFT agent to a styrene-functionalized coumarin (but with 1:1 stoichiometry) and obtained the SUMI-CTA adduct with 85% yield.<sup>28</sup> Klumperman later showed such SUMI reactions also occurred with other dithiobenzoate CTA agents and methyl acrylate,<sup>29</sup> and with vinyl acetate/*N*-vinylpyrrolidone in the presence of xanthates.<sup>30</sup> Klumperman further explored the detailed mechanism and kinetics of the SUMI reaction (or “initialization period” as referred in their works), and pointed to the importance of (a) relative stability of different radicals and (b) relative rate difference, to achieve high SUMI-CTA adduct yield.<sup>31</sup>

In 2011, Chen et al. reported the first example of SUMI between a vinylthiophene and trithiocarbonate based RAFT agent,<sup>32</sup> which later extended to styrene and *N*-isopropylacrylamide (NIPAM), including successive SUMI of styrene followed by NIPAM.<sup>23</sup> Recognizing the opportunity to create sequence-defined oligomers, other researchers have done significant works to further understand the SUMI process and its utilization, in particular, Moad,<sup>33-35</sup> Xu<sup>36-40</sup> and Junkers.<sup>41, 42</sup> Much progress has been summarized in two excellent review articles.<sup>22, 33</sup>

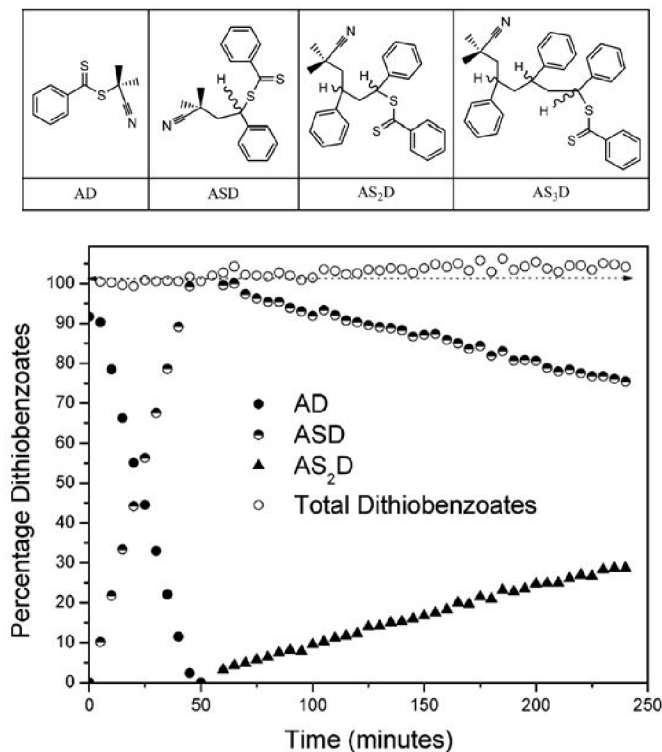


**Figure 1.** Relative concentration of dithiobenzoate species vs time in RAFT polymerization of the styrene. Reproduced with permission from ref.<sup>27</sup> Copyright 2004, with permission from American Chemical Society.

## 2.2 Choosing the appropriate pairing of monomer and CTA for RAFT step-growth

Though the process of SUMI is neither chain-growth nor step-growth by itself, such a highly efficient reaction could be harnessed using bifunctional reagents (AB type and  $A_2 + B_2$  type) of CTA and monomer to achieve step-growth polymerization. In addition to using bifunctional reagents, we would like to emphasize two key characteristic criteria to transform RAFT-SUMI process into RAFT step-growth polymerization: 1) quantitative transformation of CTA and monomer pairs into SUMI-CTA adduct under balanced stoichiometric conditions with minimal side reactions; and 2) as the polymerization proceeds through step-growth, high conversion ( $p > 0.95$ ) is necessary to obtain appreciable molecular weight (i.e., polymer). These two criteria can be fulfilled by screening a selection of CTAs for a given monomer, which has been demonstrated with maleimides and acrylic monomers as detailed below.<sup>16, 21</sup>

In the first demonstration of RAFT step-growth polymerization,<sup>16</sup> Tanaka et al. carried out the initial CTA screening with maleimides used as the monomer unit, as quantitative SUMI-CTA adduct yield was previously reported by Xu et al with CTA<sub>1A</sub>.<sup>38</sup> Using *N*-ethylmaleimide as a model monomer ( $M_1$ ), various trithiocarbonate based CTAs with different R-groups were screened (CTA<sub>1A</sub>–CTA<sub>1E</sub>). With AIBN as the external radical source, quantitative SUMI-CTA adduct yield was observed with CTA<sub>1A</sub> as expected (**Figure 2A**); however, CTA<sub>1B</sub>, which only structurally differs from CTA<sub>1A</sub> by an additional carboxylic acid (the “handle” used to conveniently create AB or  $A_2$  monomers), resulted in significantly slower kinetics (**Figure 2B**). This was attributed to slower monomer addition due to increased radical stability of this R• species contributed by the additional neighboring conjugation (i.e., COOH). Serendipitously, CTA<sub>1C</sub>,

whose reactivity lies between the former two CTA's,<sup>43</sup> was found to yield quantitative SUMI-CTA adduct yield (**Figure 2C**). In contrast, CTA<sub>1D</sub> with one less methyl substituent, resulted in significantly lower yield with a higher consumption of the monomer than the CTA (**Figure 2D**), indicative of multiple monomer addition, which was believed to be limited by the chain transfer equilibrium. Furthermore, CTA<sub>1E</sub>, which does not favor chain transfer exchange with the monomer, resulted in retarded homopolymerization (**Figure 2E**).

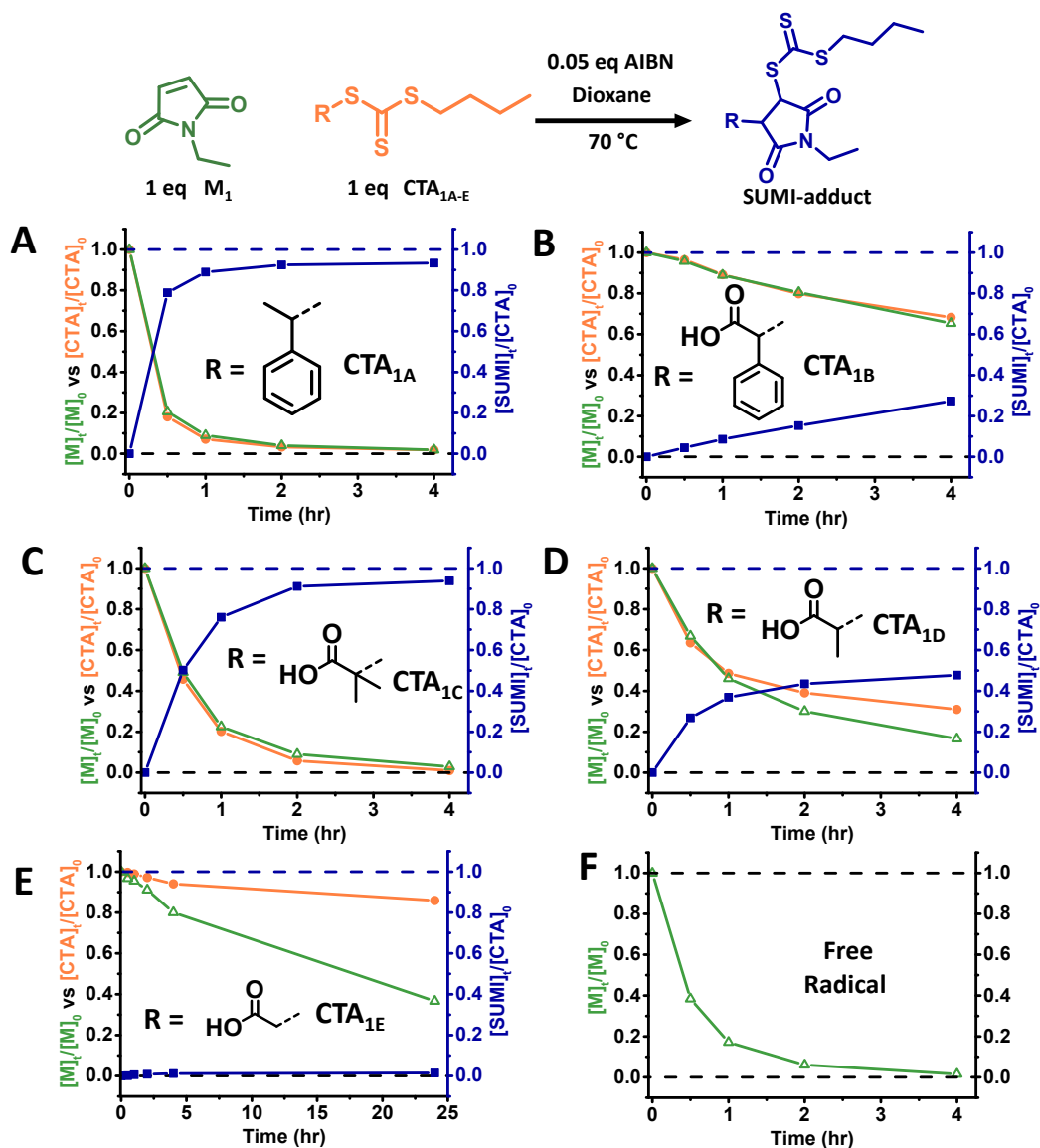


**Figure 2.** Kinetic study of RAFT-SUMI process with maleimide, where stoichiometrically equivalent amount of maleimide to CTA was used. Adapted with permission from ref.<sup>16</sup> Copyright 2021, with permission from American Chemical Society.

Compared to maleimides, acrylates are considered to be a more challenging class of monomers for RAFT step-growth process owing to the high  $k_p$  of acrylates (i.e., homopropagation, **Scheme 2**). Yet as mentioned earlier, Klumperman reported the formation of SUMI-CTA adduct of acrylates using dithiobenzoate based

CTA bearing cyano-stabilized tertiary radical fragmentation.<sup>29</sup> To expand RAFT step-growth polymerization to acrylic monomers, Archer et al. screened a selection of CTAs with butyl acrylate (BA) as the model monomer.<sup>21</sup> In their study, 4-cyano-4-(((dodecylthio)carbonothioyl)thio) pentanoic acid (CTA<sub>1F</sub>), bearing similar cyano-stabilized tertiary radical (R•), only showed limited rate of product formation (**Figure 3A**). This was attributed to the slow radical addition of the generated cyano-stabilized tertiary radical to acrylic monomer to form more reactive carbonyl ester stabilized secondary radical. Coincidentally, CTA<sub>1C</sub>, which was ultimately used for RAFT step-growth with maleimides, was observed with quantitative formation of SUMI CTA adduct with BA and equal consumption of monomer and CTA as well (**Figure 3C**).<sup>21</sup> Interestingly, CTA<sub>1B</sub> which bears intermediate reactivity between CTA<sub>1A</sub> and CTA<sub>1C</sub> in the literature,<sup>43</sup> was found to generate even lower yields than the former two CTAs (**Figure 3B**). Additionally, CTA<sub>1D</sub> and CTA<sub>1E</sub> resulted in similar characteristics to the RAFT-SUMI study with maleimides, where multiple monomer addition and retarded homopolymerization were observed, respectively (**Figure 3D-E**).<sup>21</sup>

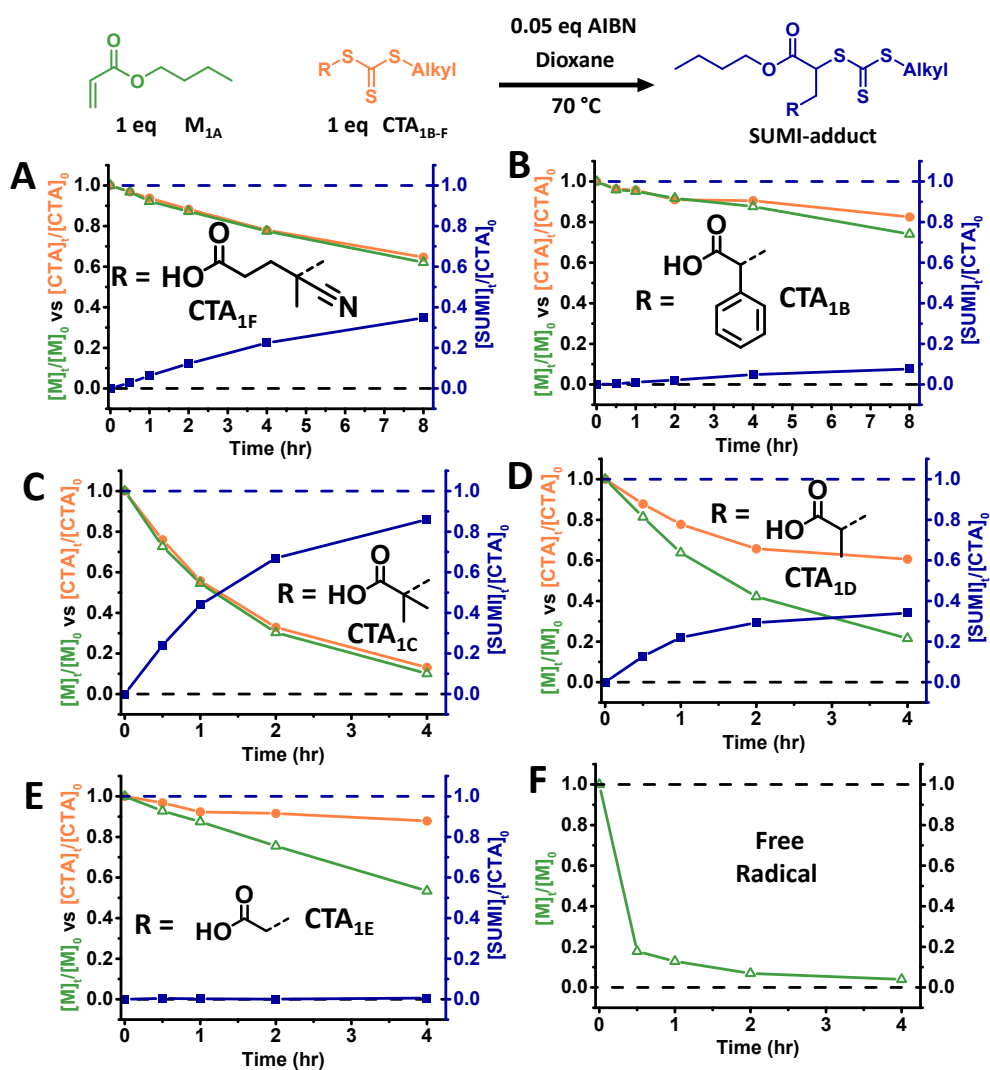


**Figure 3.** Kinetic study of RAFT-SUMI process with butyl acrylate, where stoichiometrically equivalent amount of BA to CTA was used. Adopted with permission from ref.<sup>21</sup> Copyright 2022, with permission from American Chemical Society.

### 3 Characterization of RAFT step-growth polymers

In this section, we discuss classical theoretical description of step-growth polymerization and its application in characterizing molecular weight evolution. Further details can be found in other literature sources.<sup>44</sup>

#### 3.1 Definition of molecular weight averages

Following the molecular weight evolution with monomer conversion/extent of reaction ( $p$ ) provides crucial insights into the polymerization mechanism. In contrast to proteins/DNAs where the molecular weight is a discrete value, synthetic polymers are characterized by their molecular weight averages due to the distribution of different chain lengths. Three different molecular weight averages are typically described for polymers: the number-average ( $M_n$ ), weight-average ( $M_w$ ) and Z-average ( $M_z$ ):

$$M_n = \frac{\sum M_x n_x}{\sum n_x} \quad \text{Eq 1}$$

$$M_w = \frac{\sum M_x^2 n_x}{\sum M_x n_x} \quad \text{Eq 2}$$

$$M_z = \frac{\sum M_x^3 n_x}{\sum M_x^2 n_x} \quad \text{Eq 3}$$

where  $n_x$  represents the number of a particular species ( $x$ -mer) with a defined molecular weight ( $M_x$  for  $x$ -mer). Different characterization methods provide information on one or multiple molecular-weight averages; for example, <sup>1</sup>H-NMR (via end group analysis) can be used to estimate  $M_n$ .

Size Exclusion Chromatography (SEC) analysis is typically used to characterize molecular weights of polymers, which is convenient and offers rich information based on the separation by hydrodynamic size of the polymeric species in solution (i.e., the eluent). In a SEC equipped with a differential refractometer (dRI), a molecular weight distribution can be obtained as dRI detector response is proportional to the weight concentration of the measured species.<sup>45</sup> In practice, molecular weights from SEC analysis are estimated by comparing the elution of volume of the sample polymer with known molecular weight of narrow standards (conventional SEC), or by light scattering detector (LS) which measures absolute molecular weight. Importantly, as SEC analysis measures the molecular weight distribution, all three molecular weight averages above can be determined simultaneously.

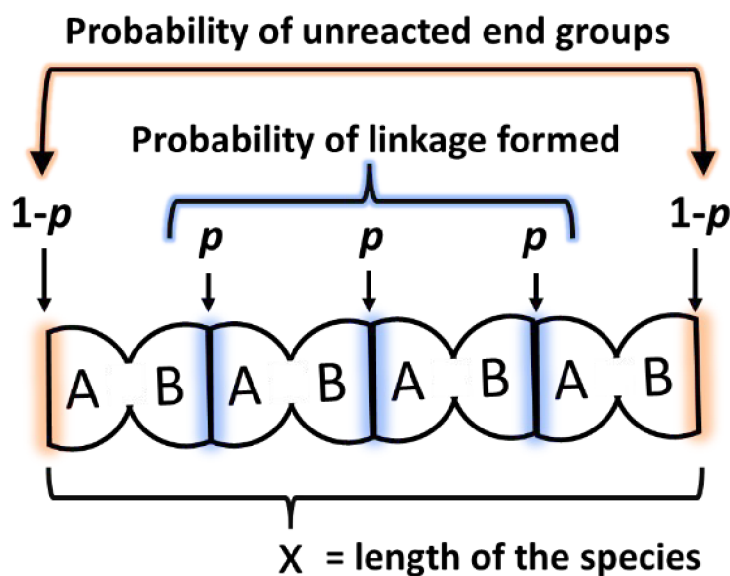
Historically, the molecular weight evolution has been characterized by following  $M_n$  and  $M_w$  with  $p$ , with the dispersity ( $\mathcal{D} = \frac{M_w}{M_n}$ ) describing the difference between these two or the breadth of the molecular weight distribution. Arguably this is acceptable for living/controlled (chain-growth) polymerization systems, where molecular weight distribution follows Poisson distribution and  $M_n$  proceeds to increase linearly with monomer conversion and  $\mathcal{D}$  is concurrently decreasing. However, following just  $M_n$  and  $M_w$  (or  $\mathcal{D}$ ) has limitations in characterizing the skewness and the shape of the molecular weight distribution. To overcome this, some attention has been given to characterizing higher moments of the molecular weight distribution such as  $M_z$ ; however it is often neglected.<sup>46</sup> In the case of step-growth polymerization, we believe that one needs to obtain all three molecular weight averages to have better and more comprehensive insights.

### 3.2 Molecular weight evolution of step-growth polymerization with balanced stoichiometry

For step-growth polymerization, Flory described the molecular weight distribution of linear step-growth polymerization in one of his classical papers.<sup>47</sup> Suppose a polymer sample has a total of  $N_0$  structural units distributed in a variety of  $x$ -mers (e.g., trimer, tetramer, etc.), and a particular  $x$ -mer has a quantity of  $n_x$  (i.e.,  $N_0 = \sum n_x x$ ). Flory started by determining the probability that a particular structural unit (A-B in **Scheme 3**) – if selected randomly from these  $N_0$  structural units – is part of an  $x$ -mer. This probability is essentially the ratio of total number of structural units in these  $x$ -mers vs. the total number of structural units ( $N_0$ ). Since each structural unit has identical molecular weight, this probability is the weight fraction of the  $x$ -mer ( $w_x$ ). On the other hand, based on a simple AB step-growth polymerization model where  $p$  represents probability of reaction between A and B occurring, and thus  $(1 - p)$  represents probability that reaction had not occurred at each end group, the probability of each particular configuration of  $x$ -mer is  $p^{x-1}(1 - p)^2$  (**Scheme 3**). Since there are  $x$  possible configurations of  $x$ -mers, the probability for any of the  $x$  configurations existing is therefore  $xp^{x-1}(1 - p)^2$ . Thus we have:

$$w_x = xp^{x-1}(1 - p)^2 \quad \text{Eq 4}$$

And the number of  $x$ -mers ( $n_x$ ) is then given by  $n_x = \frac{N_0 w_x}{x} = N_0 p^{x-1} (1 - p)^2$ .



**Scheme 3.** Illustration of the probability of  $x$ -mer formation in a step-growth polymerization. All species have two unreacted end groups.

For AB step-growth polymers, each molecular average ( $M_n$ ,  $M_w$  and  $M_z$ ) can be calculated for a given conversion ( $p$ ) by substituting  $M_x$  with  $xM_0$  ( $M_0$  is the molecular weight of the AB monomer or average molecular weight of the  $A_2 + B_2$  comonomers) and substituting  $n_x$  with the term  $N_0 p^{x-1}(1 - p)^2$ . According to the summation of the substituted terms,  $M_n$ ,  $M_w$  and  $M_z$  will become:

$$M_n = M_0 \frac{\sum xp^{x-1}(1 - p)^2}{\sum p^{x-1}(1 - p)^2} = M_0 \frac{1}{1 - p} \quad \text{Eq 5}$$

Eq 6

$$M_w = M_0 \frac{\sum x^2 p^{x-1} (1-p)^2}{\sum x p^{x-1} (1-p)^2} = M_0 \frac{1+p}{1-p}$$

$$M_z = M_0 \frac{\sum x^3 p^{x-1} (1-p)^2}{\sum x^2 p^{x-1} (1-p)^2} = M_0 \frac{1+4p+p^2}{(1-p)^2} \quad \text{Eq 7}$$

It is important to note that the molecular distribution (Eq 1) and the molecular weight averages (Eq 5-7) reflect the crude polymerization reaction mixture, accounting the initial species ( $x=1$ , i.e., monomer) but not accounting the purification process. Therefore, we emphasize that when monitoring the molecular weight evolution by SEC analysis, suitable column resolution is crucial to analyze the whole distribution of the crude polymer in order to apply these equations. It is noteworthy that molecular weight analysis by light scattering is limited due to changes of the  $dn/dc$  and insensitivity of light scattering to low molecular weight species; therefore, conventional SEC analysis is recommended when comparing experimental results with Flory's theory. Furthermore, another important consideration is that the cyclization (formation of cyclic species) is not considered in the theoretical description of Eq 4-7. Cyclization results in species with no end groups to further react, which can be considered as dead chains. Though the presence of high molecular weight cyclic species is indistinguishable from linear equivalents, oligomeric species can be observed from SEC analysis. In some cases, these species can be seen in  $^1\text{H-NMR}$  spectra due to restricted bond rotation.<sup>48</sup>

Common misconception of the step-growth polymers is that dispersity,  $D (= M_w/M_n = 1 + p)$  is 2 (when  $p$  is unity); however, this is only true in the absence of cyclization. In the cases where oligomeric cyclic species are observed, the  $M_n$  would be much lower than expected (if correctly analyzed), whereas the  $M_w$  is affected less as higher molecular species is weighted more according to its definition (Eq 3); therefore, the presence of cyclic species should result in dispersity much greater than 2. On the contrary, dispersity can be observed to be less than 2 after the removal of low molecular weight species during purification.

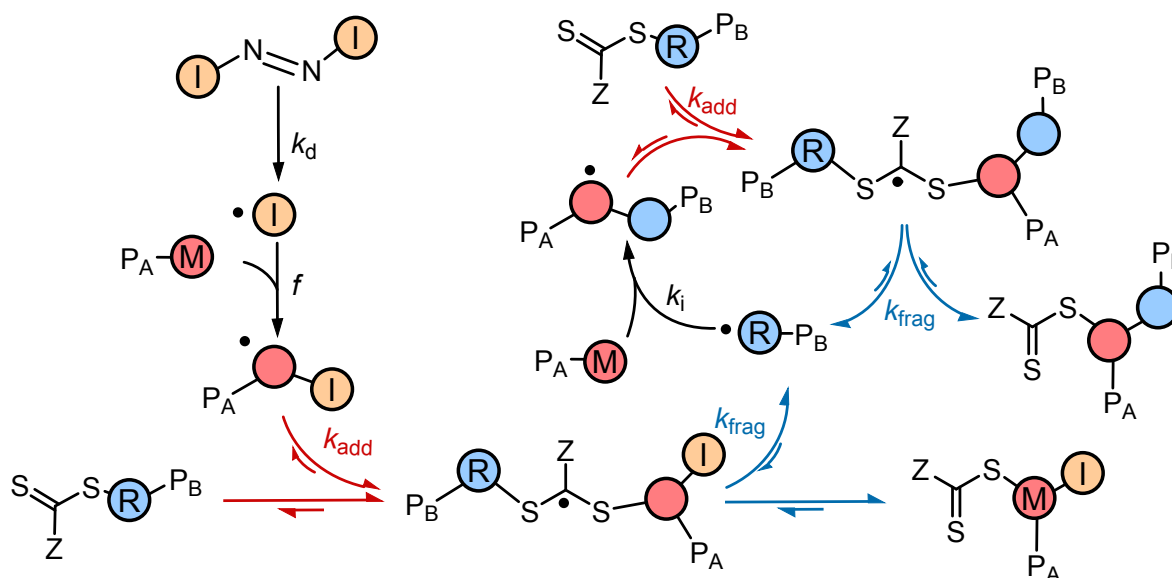
### 3.3 Accounting for imbalanced stoichiometry

The equations used for AB step-growth (Eq 4-7) can be applied directly for  $A_2 + B_2$  comonomer type step-growth with balanced stoichiometry (with  $M_0$  being the average molecular weight of the  $A_2 + B_2$  comonomers). However, with imbalanced stoichiometry, complication arises with defining molecular weight distribution and molecular weight averages due to the formation of three possible combination of end group species. Indeed, using stoichiometric excess of one comonomer (e.g.,  $B_2$ ) results in polymeric species predominantly bearing these end group species (B) at high conversion, with no counterpart (A) to react, thereby resulting in limited molecular weight. Nonetheless, the impact of the imbalanced stoichiometry on  $M_n$  can be accounted by the definition below, where  $r$  is the molar ratio of the two comonomers ( $r = N_A/N_B$ ) and it is always less than 1:

$$M_n = M_0 \frac{1+r}{1+r-2rp} \quad \text{Eq 8}$$

Though there are no simple equations to define higher order molecular weight averages ( $M_w, M_z$ ) of  $A_2 + B_2$  step-growth polymerization with imbalanced stoichiometry, it is stated that the  $p$  can be replaced with  $r^{1/2}p$  in equations 6 and 7 (except when  $r^{1/2}p \ll 1$ ) to obtain satisfactory theoretical values.<sup>47</sup>

### 3.4 Accounting for imbalanced stoichiometry from thermal initiation of diazo initiators



**Scheme 4.** Illustration of initiator derived imbalanced stoichiometry. Reproduced with permission from ref.<sup>49</sup> Copyright 2022, with permission from Royal Society of Chemistry.

Using an external initiator (such as AIBN) in the RAFT step-growth polymerization would in theory result in imbalance in stoichiometry due to the loss of one monomer functionality (**Scheme 4**). The resulting initiator-monomer adduct can be considered as a monofunctional (macro)reagent. Generally speaking, in step-growth polymerization where a monofunctional agent (e.g., B') is present, stoichiometric ratio of functional groups,  $r$  can be redefined as:<sup>44</sup>

$$r = \frac{N_A}{N_B + 2N_{B'}} \quad \text{Eq 9}$$

where  $N_A$  and  $N_B$  are the relative moles of the functional groups of the bifunctional reagents in  $A_2$  and  $B_2$  respectively, and  $N_{B'}$  is the moles of monofunctional reagent with the same functionality as  $B_2$ . A coefficient “2” is used for  $N_{B'}$  since the monofunctional reagent has the same quantitative effect in limiting the molecular weight as the excess bifunctional reagent ( $B_2$ ). Using this principle and without considering the effects from radical termination, the imbalance in stoichiometry from external initiation in the RAFT step-growth polymerization can be estimated accordingly (assuming CTA as the excess bifunctional reagent):

$$r_{\text{th}} = \frac{[M]_0}{[\text{CTA}]_0 + 4f([I]_0 - [I]_t)} \quad \text{Eq 10}$$

where  $[M]_0$  and  $[\text{CTA}]_0$  are the initial molar concentrations of monomer and CTA functional groups within the bifunctional reagents (i.e., A and B in Eq 9), whilst  $[I]_0$  and  $[I]_t$  is the molar concentration of the initiator at the beginning of the reaction and at time  $t$ . Since two radicals are generated from one molecule of azo initiator with efficiency  $f$ , to react with a monomer ( $M_2$ ) and form the initiator adduct, a factor of “4” (i.e.,  $2 \times 2$ ) is used in Eq. 10 rather than “2” in Eq 9. The initiator remaining ( $[I]_t$ ) can be calculated for specific time,  $t$ , with first-order decay with the rate constant,  $k_d$ :

$$\text{Eq 11}$$

$$[I]_t = [I]_0 e^{-k_d t}$$

The rate constant ( $k_d$ ) for the initiator decomposition can be calculated for specific temperature using the Arrhenius equation (Eq 11) from the 10-hour half-life decomposition temperature and activation energy, both of which are provided by the chemical suppliers.<sup>50</sup>

Furthermore, substituting Eq 11 into Eq 10, the overall imbalanced stoichiometry can be estimated from initial molar ratio of CTA to monomer ( $r_0 = [M]_0/[CTA]_0$ ) and initiator to monomer ( $[I]_0/[M]_0$ ):

$$r_{th} = \frac{1}{\frac{1}{r_0} + 4f \frac{[I]_0}{[M]_0} (1 - e^{-k_d t})} \quad \text{Eq 12}$$

It is important to note that the initiation efficiency is dependent on monomer and conditions. Furthermore, the key limitation in this approach (Eq 12) is the estimation of  $f$  at high monomer conversion. Typically, to account for the loss of radicals from side reactions following the thermal decomposition of the initiator, full initiation efficiency ( $f = 1$ ) is not adopted for diazo-initiators. A value of 0.65 has been recommended as the highest value for these family of initiators by Moad.<sup>51</sup> Assuming a maximum  $f$  value of 0.65 has provided relatively good agreement of experimental and theoretical  $M_w$  for RAFT step-growth polymerization for acrylates<sup>21</sup> and maleimides.<sup>16, 52</sup> However, it is important to note that the initiation efficiency  $f$  is expected to fall when monomer concentration becomes a limiting factor; thus not accounting for this fact leads to overestimation of initiator derived end groups. Therefore, assuming  $f$  to be a constant value (e.g., 0.65) leads to lower  $r_{th}$  and lower theoretical molecular weight than what should be expected, particularly when the polymerization is left for a period of time after high monomer conversion is reached whilst a relatively high abundance of remaining initiator is still present.<sup>16</sup>

### 3.5 Mark-Houwink analysis

Topology of the polymer plays significant role in the solution viscosity, as it impacts the hydrodynamic volume. Mark-Houwink analysis is a powerful tool to confirm the formation of linear polymers. Mark-Houwink equation (also known as Landau-Kuhn-Mark-Houwink-Sakurada equation) describes the relationship between intrinsic viscosity ( $[\eta]$ ) of the polymer in a solution with the molecular weight ( $M$ ) of the polymer accordingly:

$$[\eta] = KM^\alpha \quad \text{Eq 13}$$

The coefficient ( $K$ ) and exponent ( $\alpha$ ) parameter can be determined from log-log plot of intrinsic viscosity as a function of molecular weight; this plot can be obtained from multi-detector SEC analysis. The slope of this log-log plot corresponds to the  $\alpha$  parameter, which is the exponent term for evolution of intrinsic viscosity with molecular weight. Typically for linear polymers, this value is between 0.5 to 0.8, depending on the solvent interaction and flexibility of the polymer backbone. In contrast, branched polymers exhibit lower intrinsic viscosity relative to their molecular weight due to their more compact hydrodynamic radius and yield  $\alpha$  values less than 0.5.<sup>53</sup>

#### 4. RAFT step-growth with More Activated Monomers (MAMs)

In this section we will focus on RAFT step-growth polymerization with More Activated Monomers (MAMs), which are a class of monomers where the vinyl group is conjugated with radical stabilizing moieties such as aromatics and esters. MAMs typically include styrene, (meth)acrylates, (meth)acrylamides, among others. To date, RAFT step-growth polymerization has been demonstrated with two families of MAMs, acrylate and maleimides.

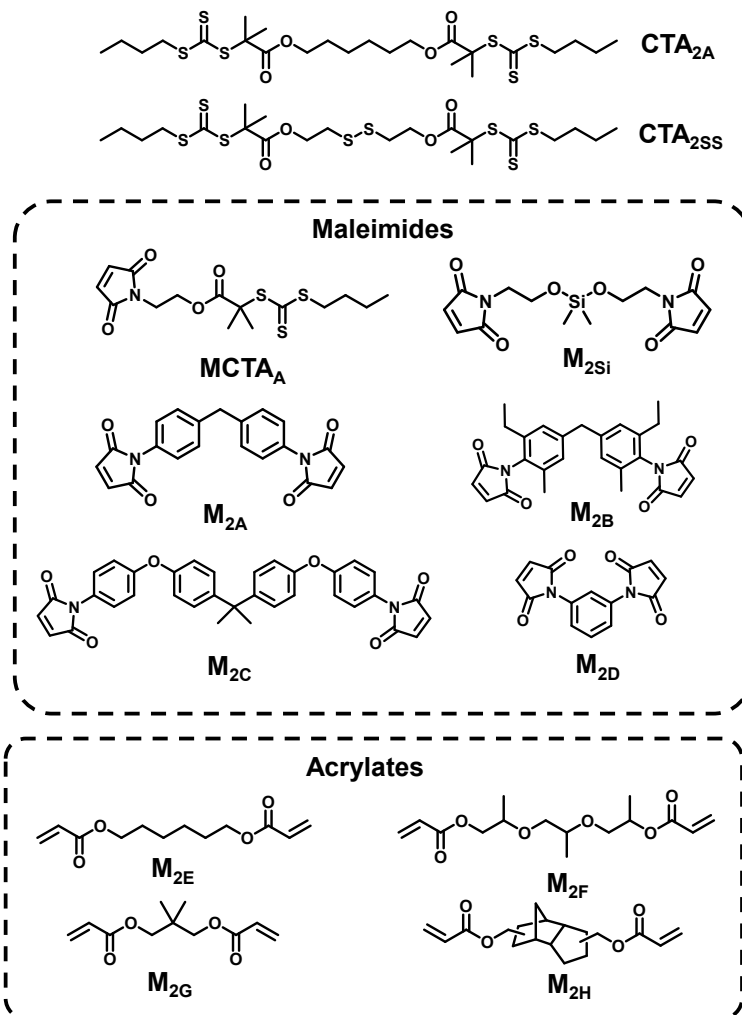


**Chart 1.** More activated monomers (MAMs) in RAFT step-growth

##### 4.1 RAFT step-growth with maleimides

Having a more reactive vinyl group, MAMs typically can readily homopolymerize (high  $k_p$ ), which is not ideal for RAFT step-growth. Therefore, the first report on RAFT step-growth focused on maleimides since maleimides are known to bear low  $k_p$ . As mentioned earlier,  $CTA_{1C}$  was found to yield quantitative SUMI-CTA adduct with model maleimide monomer; thus tethering the two functionalities together,  $MCTA_A$  (structure in **Chart 1**) was designed to be the first AB type RAFT step-growth monomer.<sup>16</sup> Successful RAFT AB step-growth polymerization was observed, manifested by the evolution of molecular weight averages with conversion following predicted step-growth molecular weight averages from Eq 5, 6 and 7

(Figure 4A). However, the low molecular weight cyclic species (formed during the polymerization) resulted in significant deviation of  $M_n$  from ideal step-growth molecular weight evolution. Nonetheless, the higher order molecular weight averages such as  $M_w$  and  $M_z$  gave more reasonable agreement. It should be noted that, by further considering the imbalanced stoichiometry due to exogenous initiator ( $\zeta_{th} = 0.949$ , Eq 12, Table 1), the theoretical  $M_w$  ( $M_{w,th} = 18k$ , Table 1) was much closer to the experimental value ( $M_w = 9.9k$ , Table 1) than the experimental value without considering initiation ( $M_{w,th} = 49k$ , Table 1). Furthermore, polymerization conducted at higher concentration of AB monomers was found to be optimal for yielding higher molecular weight polymers with lower initiator equivalence, whereas lowering the initial concentration of the polymerization resulted in more noticeable presence of the cyclic species, which is a classical step-growth feature. Surprisingly, despite the high tolerance of RAFT process, conducting this particular RAFT step-growth polymerization in DMSO or DMF had undesirable loss of control, which was not observed when using toluene or dioxane as the solvent; this unusual behavior was speculated to be side reactions of maleimide monomers in polar solvents.

In the same report,<sup>16</sup> Tanaka et. al. further investigated the RAFT step-growth polymerization with  $A_2 + B_2$  type comonomers using bifunctional pairs of monomers ( $M_{2Si}$ ) and CTA ( $CTA_{2A}$ ). Compared to the AB type step-growth, lower fraction of cyclic species was observed as the probability of the chain ends to cyclize is reduced by a factor of two, resulting in better agreement of  $M_n$ ,  $M_w$  and  $M_z/M_w$  with expected values (Figure 4B). Additionally, using excess bifunctional CTA to limit the molecular weight was successfully demonstrated. Furthermore, using Eq 12 to estimate the overall imbalance of stoichiometry, the theoretical  $M_w$  values were significantly closer to the experimental values across a range of different stoichiometric ratios of CTA and monomer (Table 1). Finally, Mark-Houwink analysis of both AB and  $A_2 + B_2$  step growth polymers revealed an  $\alpha$  value of 0.6 (Figure 4C), consistent with solution behavior of linear polymers.

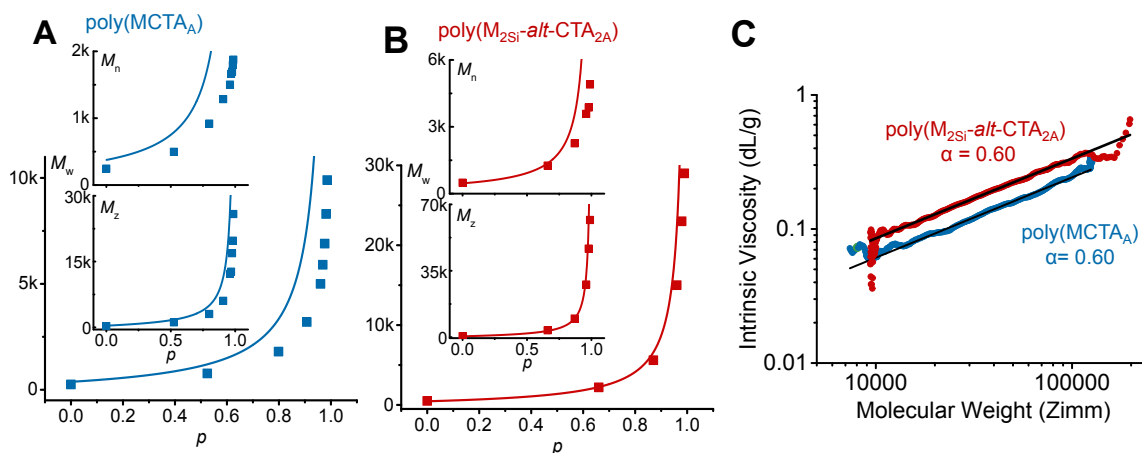


**Figure 4.** Molecular weight evolution of the first AB and  $A_2 + B_2$  RAFT step-growth and Mark-Houwink plot of the isolated polymers. Adapted with permission from ref.<sup>16</sup> Copyright 2021, with permission from American Chemical Society.

The main drawback to the original report was the difficulty in preparing maleimide based monomers, which required multiple synthetic steps, limiting the overall utility and scalability. To overcome this problem, Boeck et al. explored the use of commercially available and affordable *N*-aromatic bismaleimides.<sup>52</sup> Successful RAFT step-growth polymerization was demonstrated with *N,N'*-(1,4-phenylene)dimalimide,

$M_{2A}$  together with  $CTA_{2A}$  (**Chart 1**), as the evolution of molecular weight averages with monomer conversion tracked well with predicted values (**Figure 5A**). Similar to the original report, Eq 12 was found to be effective in predicting the overall imbalance of stoichiometry (**Table 1**). Additionally, given the affordability of  $M_{2A}$  (0.59 \$/g), polymerization at multigram scale was reported with successfully isolating 8.1 grams (81 % yield) of  $P(M_{2A}\text{-}i\text{t}\text{-}CTA_{2A})$  (**Figure 5F**).

Bis(3-ethyl-5-methyl-4-maleimidophenyl) methane ( $M_{2B}$ , **Chart 1**) and 2,2-bis[4-(4-maleimidophenoxy)phenyl]propane ( $M_{2C}$ , **Chart 1**) that were structurally analogous to  $M_{2A}$ , also demonstrated successful RAFT step-growth polymerization (**Figures 5B, 5C**), however, with contrasting kinetics. The polymerization of  $M_{2B}$ , having alkyl ortho-substituents, was considerably slower in rate; however, SEC analysis disclosed noticeably less oligomeric cyclic species, yielding  $D$  values of the reaction mixture closer to the expected value of 2 for step-growth. It was speculated that the steric hindrance in  $M_{2B}$ , imparted by the alkyl-substituents, would reduce the rate of the end group addition (i.e.,  $R\cdot$  to  $M$ ) and thus result a lower rate of polymerization; however, the same steric hindrance would also reduce the flexibility of the linear polymeric chain and lower the probability of cyclization to occur. On the other hand,  $M_{2C}$ , bearing O-phenyl substituent *para* to the maleimide unit, was reported to reach high conversion ( $p = 0.995$ ) and high molecular weight after just 2 hours using the same reaction conditions, suggesting the O-phenyl substituent *para* to the maleimide unit increases the monomer reactivity. It is important to note that  $M_z/M_w$  values were also higher than expected, suggesting some deviation from linear step-growth molecular weight evolution due to possible branching.

4,4 substituted phenylene bismaleimide,  $M_{2D}$  (**Chart 1**), which bears maleimide substituents attached on the same aromatic ring, was able to reach high conversion within 4 hours in *m*-cresol ( $p = 0.967$ ); however, relatively lower  $M_n$  was observed (**Figure 5D**), owing to the noticeably higher presence of oligomeric cyclic species by SEC, likely promoted by proximity and orientation of the maleimide units on  $M_{2D}$ .

Finally, it is worth noting that Mark-Houwink analysis confirmed linear topology (**Figure 5E**) for the RAFT step-growth polymers from all the commercially bismaleimides investigated (**Chart 1**).

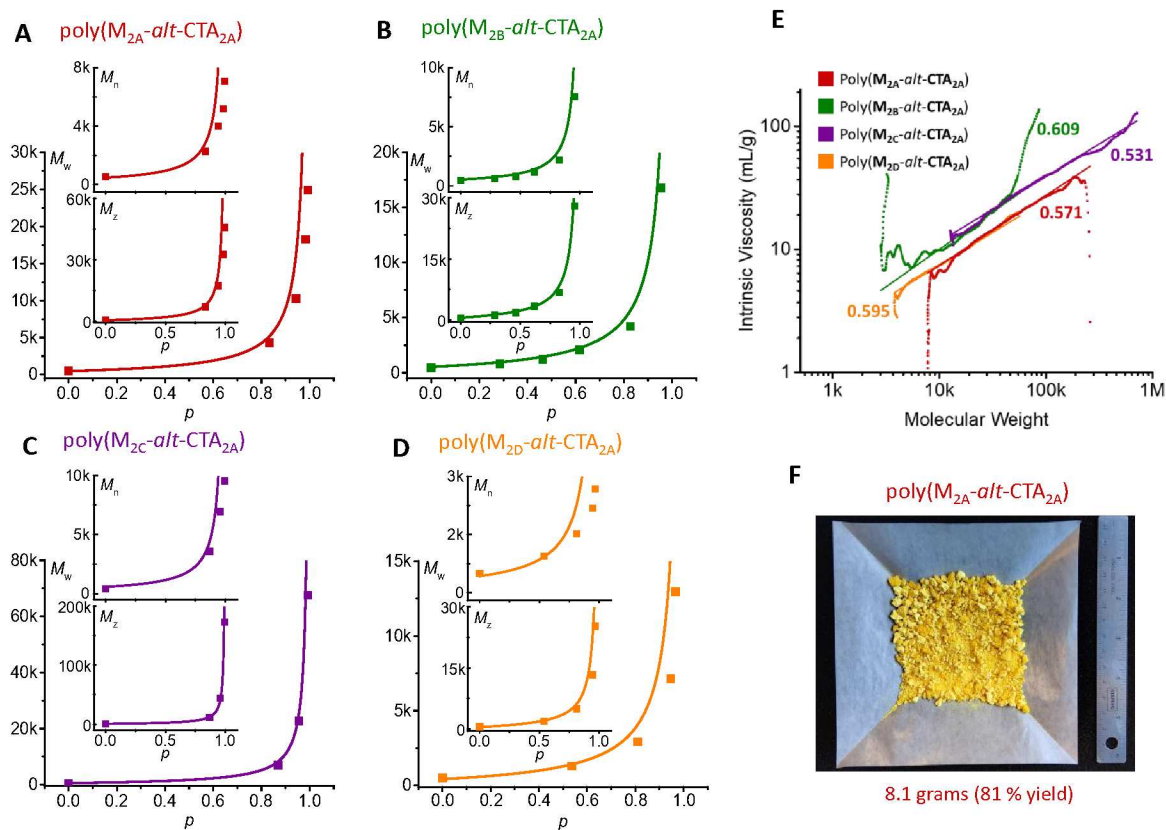


**Figure 5.** Molecular weight evolution of RAFT step-growth with commercially available bis-maleimides and Mark-Houwink plot of the isolated polymers. Upscaled synthesis of  $\text{P}(\text{M}_{2A}\text{-alt-CTA}_{2A})$ . Adapted with permission from ref.<sup>52</sup> Copyright 2022, with permission from Royal Society of Chemistry.

**Table 1.** RAFT step-growth polymerization with maleimides

Entry	Structure <sup>a</sup>	$p$ <sup>b</sup>	$r_{th}$ <sup>c</sup>	$M_{w,th}$ <sup>d</sup>	$M_{w,th} (r_{th})$ <sup>e</sup>	$M_{w,SEC}$ <sup>f</sup>	$M_w/M_n$ <sup>f</sup>	$M_z/M_w$ <sup>f</sup>
1	Poly(MCTA <sub>A</sub> )	0.985	0.949	49k	18k	9.9k	5.28	2.61
2	Poly(M <sub>2Si</sub> - <i>alt</i> -CTA <sub>2A</sub> )	0.989	0.949	84k	25k	29k	5.92	2.13
	( $r_0 = 0.98$ ) <sup>g</sup>	0.975	0.929	26k	15k	12.4k	3.66	1.83
	( $r_0 = 0.96$ ) <sup>g</sup>	0.972	0.912	19k	12.5k	11.4k	4.13	1.87
	( $r_0 = 0.934$ ) <sup>g</sup>	0.983	0.881	18.3k	11.6k	8k	3.08	1.77
	( $r_0 = 0.818$ ) <sup>g</sup>	0.983	0.780	8.0k	6.6k	5.2k	2.67	1.75
3	Poly(M <sub>2A</sub> - <i>alt</i> -CTA <sub>2A</sub> )	0.993	0.949	134k	28k	24.9k	3.52	1.83
	( $r_0 = 0.98$ ) <sup>g</sup>	0.994	0.930	59k	23k	20.2k	3.08	1.74
	( $r_0 = 0.935$ ) <sup>g</sup>	0.996	0.889	25k	15k	13.7k	2.88	1.71
	( $r_0 = 0.818$ ) <sup>g</sup>	0.998	0.782	9.4k	7.6k	8.0k	2.32	1.65
4	Poly(M <sub>2B</sub> - <i>alt</i> -CTA <sub>2A</sub> ) <sup>h</sup>	0.942	0.891	23k	9.3k	13.1k	2.16	1.73
5	Poly(M <sub>2C</sub> - <i>alt</i> -CTA <sub>2A</sub> ) <sup>i</sup>	0.992	0.970	144k	50k	56k	5.11	2.12
6	Poly(M <sub>2D</sub> - <i>alt</i> -CTA <sub>2A</sub> )	0.967	0.949	25.5k	14k	13k	4.85	1.95

- Unless stated otherwise, all reactions are carried out under the same conditions ( $[M_2]_0 : [CTA_2]_0 : [AIBN]_0 = 0.5 \text{ M} : 0.5 \text{ M} : 0.05 \text{ M}$ ) at 70 °C for 4 hours.
- Conversion determined by <sup>1</sup>H-NMR.
- Theoretical estimate (from Eq. 12) of the imbalanced stoichiometry taking initiator into consideration
- Theoretical  $M_w$  (from Eq. 6) without considering initiation.
- Theoretical  $M_w$  considering imbalanced stoichiometry (from Eq 12) by replacing  $p$  with  $r_{th}^{1/2}p$  in Eq 6.
- Experimental obtained from SEC analysis
- Polymerization carried out with excess CTA ( $r_0 = [M]_0/[CTA]_0$ ).
- After 21 hours of polymerization
- After 2 hours of polymerization

## 4.2 RAFT step-growth with acrylates

As discussed above, limiting homopropagation is crucial to avoid the possible branching via multiple monomer addition; therefore, intuitively high  $k_p$  monomers are less ideal. Yet high  $k_p$  monomers such as acrylates have been observed to undergo selective initialization period (SUMI process) <sup>29</sup> due to higher chain transfer efficiency of certain RAFT agents. Interestingly, the same CTA (CTA<sub>1c</sub>) previously employed with maleimides, also found potential utility to achieve RAFT step-growth with acrylic monomers (see **section 2.2**). In contrast to maleimides, acrylates are a class of monomers that are synthetically easy to prepare. Furthermore, compared to bis-maleimides, there is an even greater diversity of inexpensive and commercially available diacrylates.

Archer et al. successfully achieved RAFT step-growth polymerization of acrylates by using CTA<sub>2A</sub> and hexanediol diacrylate as a model monomer (M<sub>2E</sub> in **Chart 1**), reaching high conversion ( $p = 0.98$ ) after 4 hours with step-growth molecular weight evolution (**Figure 6A**). In contrast to maleimides, RAFT step-

growth polymerization of diacrylates was not affected by polar solvents such as DMF and DMSO. Interestingly, the rate was maintained when changing the concentration of the polymerization (but keeping the initiator concentration constant); by contrast, changing concentration of the initiator (but keeping its equivalence to CTA constant) resulted in a dramatic effect in rate. These results are different from traditional RAFT chain-growth kinetics, where the rate is often dependent on the ratio of CTA to initiator according to the intermediate termination model,<sup>54</sup> which is typically observed for relatively stable RAFT intermediate described in RAFT main equilibrium (degenerative chain transfer). The rate dependence of CTA to initiator ratio was not observed in these reported RAFT step-growth systems (maleimides and acrylates discussed here), is likely due to the rapid fragmentation of the R• group.

A library of polymer backbones was successfully prepared from other commercially available diacrylate monomers ( $M_{2F-H}$ ) under the same reaction conditions, and all maintained step-growth molecular weight evolution (**Figure 6B-E**) Furthermore, Mark-Houwink analysis of the diacrylate RAFT step-growth polymers (**Figure 6F**) revealed exponent parameters of 0.5–0.72, consistent with the expected linear polymers. It is worth noting that, compared to bismaleimides, the experimental  $M_w$  were typically lower than the expected values despite taking imbalanced stoichiometry from initiation into account (**Table 2**).

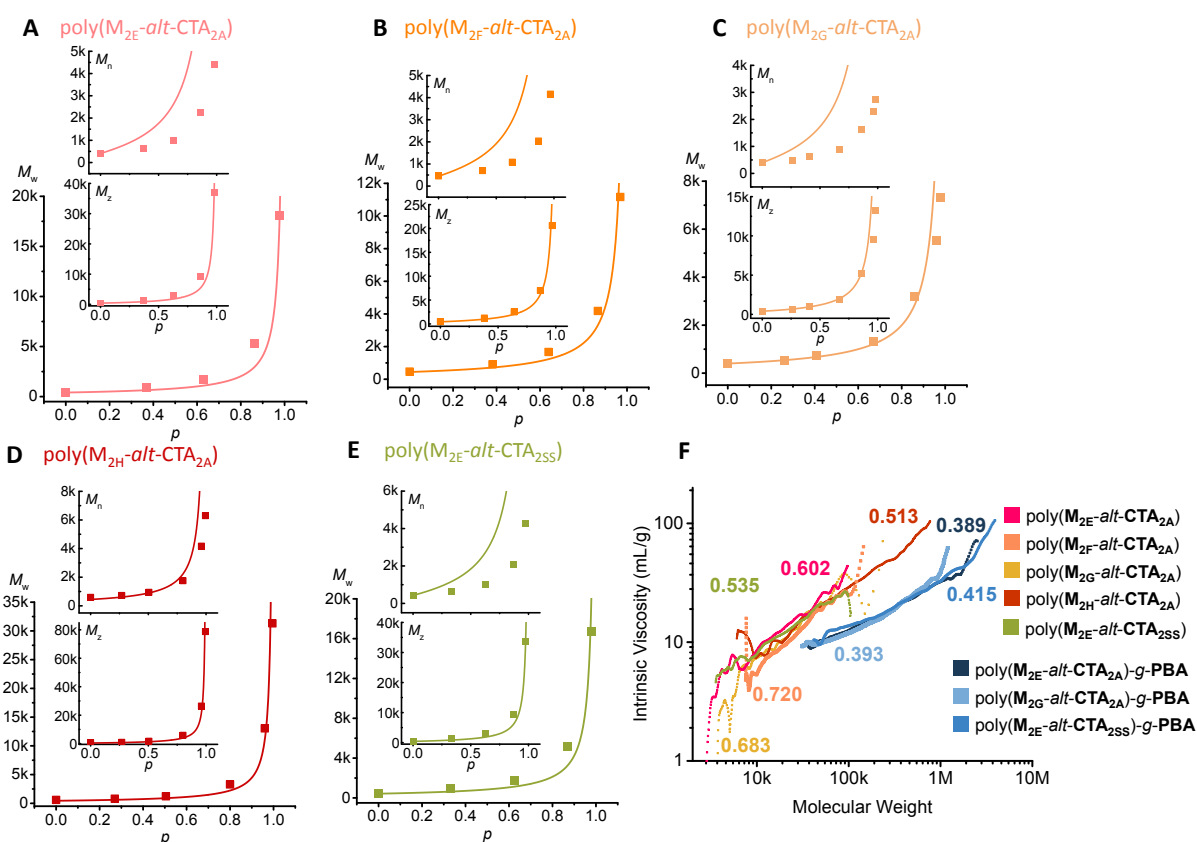


**Figure 6.** Molecular weight evolution of RAFT step-growth with commercially available diacrylates and Mark-Houwink plot of the isolated polymers and graft copolymers. Adapted with permission from ref.<sup>21</sup> Copyright 2022, with permission from American Chemical Society.

**Table 2.** RAFT step-growth polymerization with diacrylates

Entry	Structure <sup>a</sup>	$p$ <sup>b</sup>	$r_{th}$ <sup>c</sup>	$M_{w,th}$ <sup>d</sup>	$M_{w,th} (r_{th})$ <sup>e</sup>	$M_{w,SEC}$ <sup>f</sup>	$M_w/M_n$ <sup>f</sup>	$M_z/M_w$ <sup>f</sup>
1	Poly(M <sub>2E</sub> - <i>alt</i> -CTA <sub>2A</sub> )	0.980	0.974	90k	36.3k	18.0k	4.10	2.06
2	Poly(M <sub>2F</sub> - <i>alt</i> -CTA <sub>2A</sub> )	0.969	0.974	28.2k	19.8k	11.2k	2.68	1.85
3	Poly(M <sub>2G</sub> - <i>alt</i> -CTA <sub>2A</sub> )	0.98	0.974	39.6k	23.8k	7.3k	2.69	1.80
4	Poly(M <sub>2H</sub> - <i>alt</i> -CTA <sub>2A</sub> )	0.995	0.974	178k	48.6k	31.3k	4.97	2.51
5	Poly(M <sub>2E</sub> - <i>alt</i> -CTA <sub>2SS</sub> )	0.978	0.974	42.0k	25.3k	16.8k	3.93	2.02

- Unless stated otherwise, all reactions are carried out under the same conditions ( $[M_2]_0 : [CTA_2]_0 : [AIBN]_0 = 1.0 \text{ M} : 1.0 \text{ M} : 0.05 \text{ M}$ ) at 70 °C for 4 hours.
- Conversion determined by <sup>1</sup>H-NMR.
- Theoretical estimate (from Eq. 12) of the imbalanced stoichiometry taking initiator into consideration
- Theoretical  $M_w$  (from Eq. 6) without considering initiation.
- Theoretical  $M_w$  considering imbalanced stoichiometry (from Eq 12) by replacing  $p$  with  $r_{th}^{1/2}p$  in Eq 6.
- Experimental obtained from SEC analysis

## 5 RAFT step-growth polymerization with Less Activated Monomers (LAMs)

Less Activated Monomers (LAMs) are a class of unconjugated monomers (e.g., vinyl esters, vinyl amides, vinyl imides, allyl monomers, etc.) that bear less reactive vinyl bond towards radical reaction. Typically, these LAMs exhibit low  $k_p$  values or cannot be readily homopolymerized through radical mechanism ( $k_p \sim 0$ ), thus favoring the formation of RAFT-SUMI adduct and suitable for RAFT step-growth polymerization (*vide supra*).

### 5.1 RAFT step-growth polymerization with vinyl ethers

The first RAFT-SUMI reaction between LAMs and xanthates was demonstrated by Zard and coworkers in 1988 (**section 2.1**);<sup>24</sup> however, this early discovery was not utilized to achieve RAFT step-growth polymerization until 2022, when Li and Zhu reported the RAFT step-growth polymerization with a vinyl ether and a xanthate CTA bearing secondary carboxylate.<sup>55</sup> Successful step-growth polymerization was demonstrated with both AB type (MCTA<sub>B</sub> in **Figure 7**) and A<sub>2</sub> + B<sub>2</sub> type step-growth monomers (M<sub>2I</sub> and CTA<sub>2B</sub> in **Figure 7**) using photo-iniferter (initiator, chain transfer agent, and terminator, *vide infra*) conditions. However, the polymerization rate was much slower when compared with the polymerizations using MAMs, even under thermally initiated conditions with AIBN.<sup>55</sup> Nonetheless, evolution of all three molecular weight averages indicated the successful step-growth (**Figure 7A-B**).

### 5.2 RAFT step-growth polymerization with allylic monomers

More recently, the same group further expanded the monomer scopes for RAFT step-growth polymerization to allylic monomers (**Figure 7**).<sup>56</sup> Efficient formation of RAFT-SUMI adduct was observed using previously employed xanthate based CTA with stoichiometrically equivalent 1-hexene as the model monofunctional monomer. RAFT step-growth polymerization was then successfully carried out with a series of bifunctional allyl monomers and the xanthate CTA, indicated by the evolution of molecular weight averages with conversion (**Figure 7C-F**). Furthermore, the polymerization rate decreased in the order of  $M_{2J} > M_{2K} > M_{2L} \approx M_{2M}$ , which was attributed to the decreased monomer activities for radical addition reaction.

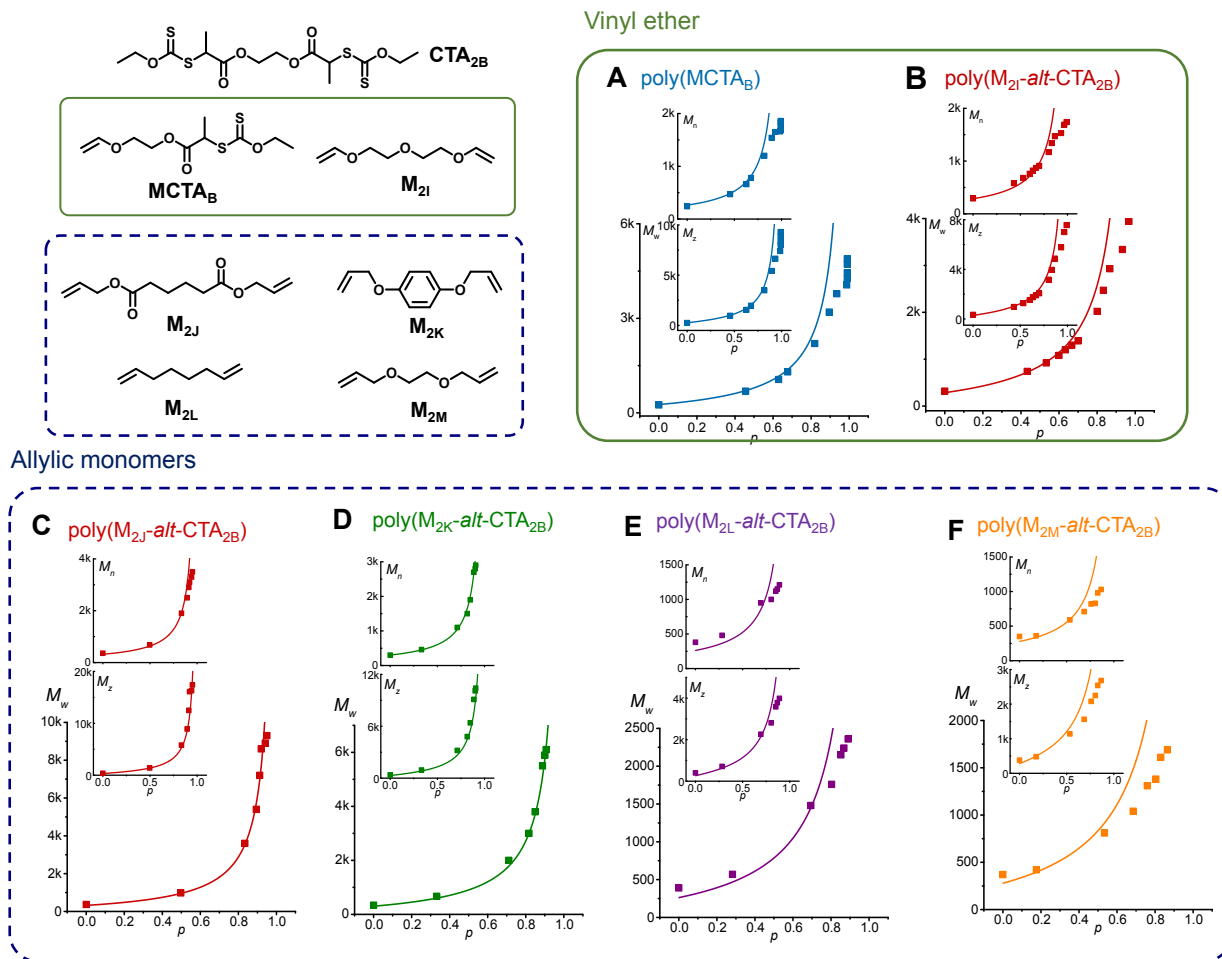


**Figure 7.** Molecular weight evolution of the RAFT step-growth with LAMs. Adapted with permission from ref.<sup>55, 56</sup> Copyright 2022 and 2023, with permission from American Chemical Society and Wiley.

## 6 Light-mediated RAFT step-growth polymerization

### 6.1 Photo-iniferter RAFT step-growth polymerization

Photo-mediated polymerizations provide various benefits, including spatiotemporal control, support of greener practices, and use of mild conditions.<sup>57</sup> Historically, thiocarbonylthio compounds have been used to generate radicals under irradiation and initiate polymerization without the use of exogenous radical sources,<sup>58</sup> even before the discovery of RAFT polymerization. This was first demonstrated by Otsu who termed this concept as iniferter (now commonly referred to as photo-iniferter).<sup>58</sup> After the discovery of RAFT polymerization, numerous photo-iniferter polymerization using common RAFT agents were reported with UV-light and gamma radiation.<sup>59, 60</sup> Mechanistically, the direct photo-cleavage of the RAFT agent can occur by accessing the  $\pi$ - $\pi^*$  symmetry allowed transition, which requires UV irradiation. More recently, by exploiting specific RAFT agents that absorb light in the visible region, RAFT-iniferter was extended to visible light by accessing n- $\pi^*$  symmetry (or dipole) forbidden transition.<sup>61-64</sup>

Photo-iniferter was recently applied to RAFT step-growth as well,<sup>49, 65</sup> where initiation can occur through two possible activation pathways, either via the end group CTA (**Figure 8A**, Activation pathway I) or backbone CTA (**Figure 8A**, Activation pathway II), generating radical intermediates in the RAFT step-growth cycle.<sup>49</sup>

## A RAFT-Iniferter Step-Growth Polymerization

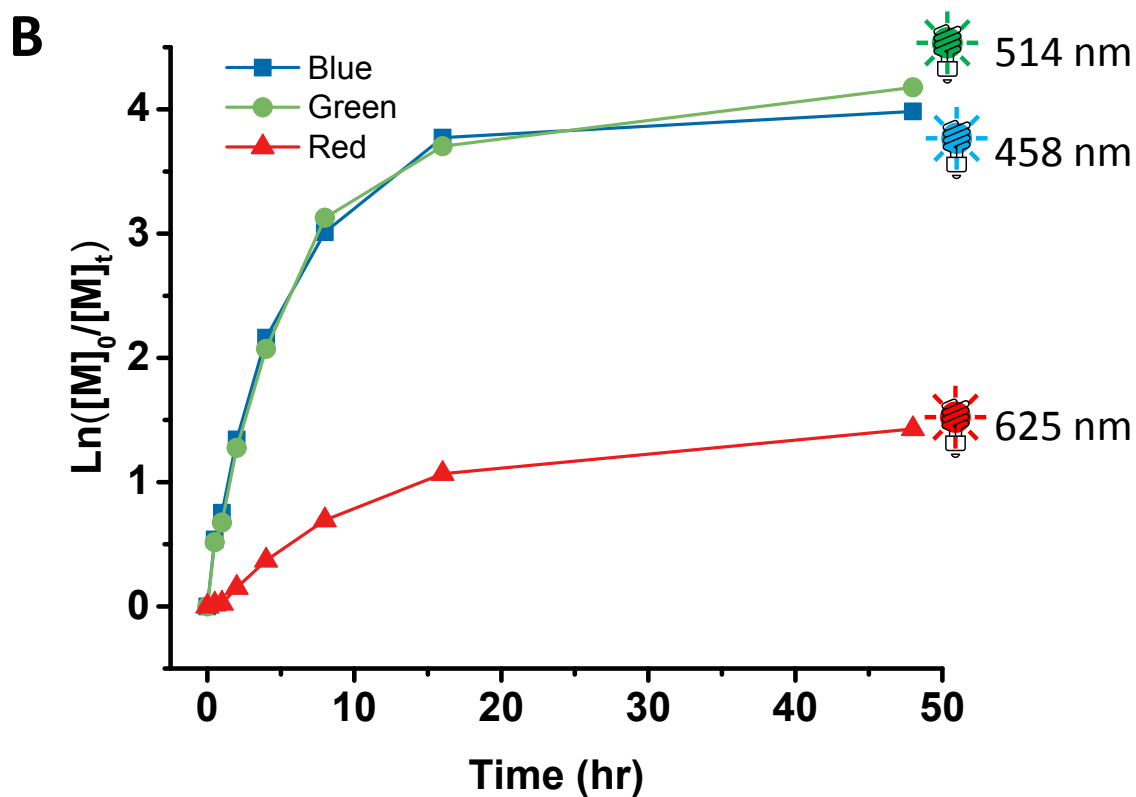
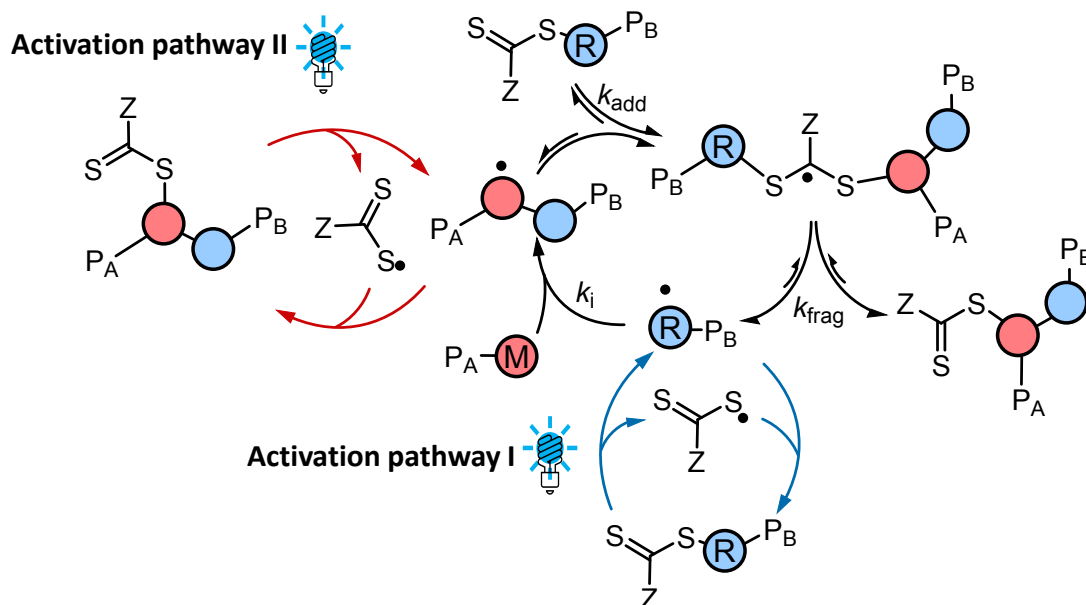


**Figure 8.** A) Illustration of RAFT-iniferter step-growth mechanism and B) semi-logarithmic plot. Adapted with permission from reference.<sup>49</sup> Copyright 2022, with permission from Royal Society of Chemistry.

In one report,<sup>49</sup> Clouthier et al. employed a bifunctional maleimide monomer ( $M_{2A}$ ) and bifunctional trithiocarbonate based RAFT agent ( $CTA_{2A}$ ) to attempt the RAFT step-growth polymerization under blue, green, and red light. The polymerization proceeded to high conversion under blue and green light conditions ( $p > 0.98$ ); however, under red light, the polymerization reached low conversion and molecular weight ( $p = 0.76$ ,  $M_w = 3.1k$ ), which was attributed to the minimal overlap of the CTA with the red LED emission spectra. Nevertheless, the polymerization proceeded with step-growth molecular weight evolutions for all three wavelengths. Interestingly, fitting the kinetics of the polymerization with a semi-logarithmic plot presented a plateau, indicating a deviation from first order kinetics. This deviation was attributed to the fact that the tertiary radical (from end group CTA) is more stable than the secondary radical (from backbone CTA), resulting in preference of photo-fragmentation of the end group CTA (Activation pathway I). Although kinetics vary between photo-reactor conditions,<sup>66</sup> Aerts et al. also observed a similar trend in RAFT-iniferter SUMI system for green and blue light conditions, where a plateau in the semi-logarithmic plot occurred at higher conversion ( $p > 0.65$ ); this was attributed to SUMI-CTA adduct absorbing light at the expense of the initial CTA.<sup>35</sup>

In another report,<sup>55</sup> Li et al. demonstrated a temporal control of RAFT-iniferter AB step-growth with  $MCTA_B$  by conducting photochemical “on/off” experiments, where the polymerization halted in the dark (“off” phase) and continued to proceed under the presence of light (“on” phase, **Figure 9**). Additionally, owing to the oil state of the  $MCTA_B$ , direct bulk polymerization was demonstrated.<sup>55</sup>

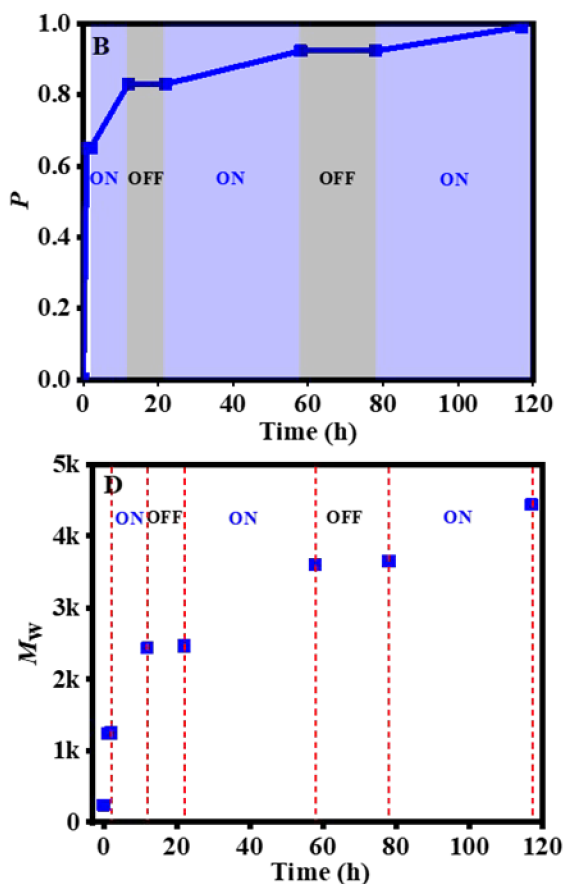


**Figure 9.** Demonstration of temporal control with RAFT iniferter step-growth. Adapted with permission from reference.<sup>55</sup> Copyright 2022, with permission from American Chemical Society.

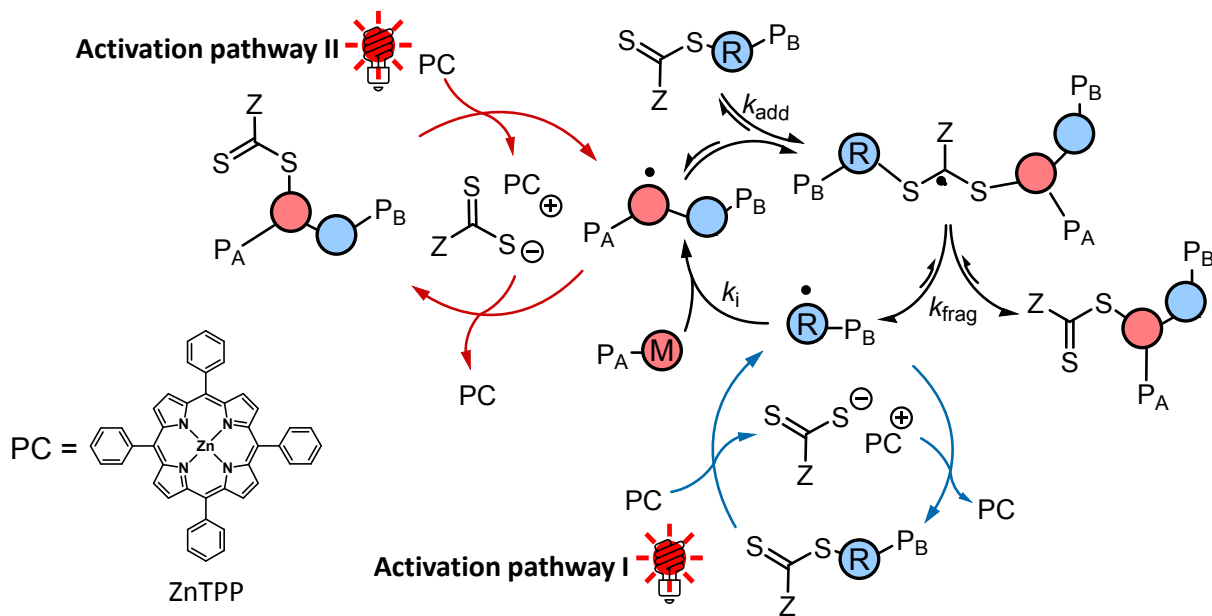
## 6.2 PET-RAFT step-growth polymerization

In contrast to RAFT-iniferter, where the light directly fragments the CTA, another related technique recently emerged proceeds via photo-induced electron/energy transfer (PET), where photo-excited photocatalyst fragments the CTA upon transfer of an electron or triplet energy to a CTA.<sup>67</sup> The initial PET-RAFT (chain-growth polymerization) was implemented with an iridium based photocatalyst (*fac*-Ir(ppy)<sub>3</sub>) to polymerize a wide range of conjugated and unconjugated monomers from various CTAs.<sup>68</sup> PET-RAFT was then extended to aqueous media using a water-soluble ruthenium based photocatalyst (Ru(bpy)<sub>3</sub><sup>2+</sup>) to polymerize a wide range of MAMs.<sup>69</sup> In a more recent study, the specific initiation mechanism of these two catalysts (*fac*-Ir(ppy)<sub>3</sub> and Ru(bpy)<sub>3</sub><sup>2+</sup>) was proposed to proceed through triplet energy transfer.<sup>70</sup> Moreover, zinc centered metalloporphyrin based catalyst has been highly attractive for PET-RAFT with trithiocarbonates based CTAs;<sup>71</sup> in particular, due to its low cost and oxygen tolerance, zinc tetraphenylporphyrin (ZnTPP) has been utilized by many researchers.<sup>72</sup> Additionally, various organic based photocatalysts have been explored for PET-RAFT.<sup>73</sup>

Recently, Clouthier et al. demonstrated the PET-RAFT step-growth polymerization of a bismaleimide monomer (M<sub>2A</sub>) and CTA<sub>2A</sub>, with ZnTPP as the photocatalyst under blue, green, and red-light conditions.<sup>49</sup> In contrast to photo-iniferter RAFT step-growth, the mechanism is proposed to occur with thiocarbonylthiolate anion fragmentation (**Figure 10A**, Activation pathway I/II), which has been speculated to have higher stability than thiocarbonylthiyl radical and therefore would improve the chain end fidelity.<sup>74</sup> The polymerization proceeded to high conversion with step-growth molecular weight evolution, under all three different wavelengths. However, the initial rates for PET-RAFT step-growth (under blue and green light) were slower than the catalyst free conditions (i.e., RAFT-iniferter step-growth, **Figure 8B**); this observation contrasts traditional RAFT chain-growth kinetics where PET-RAFT was faster than RAFT-iniferter.<sup>75</sup> Nonetheless, the polymerization proceeded under pseudo-first order kinetics with respect to monomer under all three light conditions (**Figure 10B**), indicating constant reactive radical intermediates throughout the polymerization, which is consistent with reported PET-RAFT kinetics.<sup>36, 76</sup> However, the kinetics for PET-RAFT step-growth showed a slight deviation from linearity of the semi-logarithmic plot at high conversion (**Figure 10B**), which was attributed to the preference for photo-fragmentation of the end group CTA (**Figure 10A**, Activation pathway I).<sup>49</sup>

Although photo-mediated RAFT step-growth polymerizations was expected to provide higher molecular weights by eliminating the possible stoichiometric imbalance from thermal initiators, Clouthier et al. did not observe this improvement in molecular weight, which was attributed to monomer impurity and difficulty in achieving stoichiometric balance. To further investigate end-group fidelity of photo-mediated RAFT step-growth, the authors employed an AB type monomer, which by nature is stoichiometrically balanced, to polymerize via PET-RAFT step-growth. Yet a difference of a factor of two between the theoretical and experimental molecular weight ( $M_{w,th} = 70k$ ,  $M_w = 30k$ ) was still observed, which was attributed to the formation of cyclic species.<sup>49</sup>

## A PET-RAFT Step-Growth Polymerization



## B

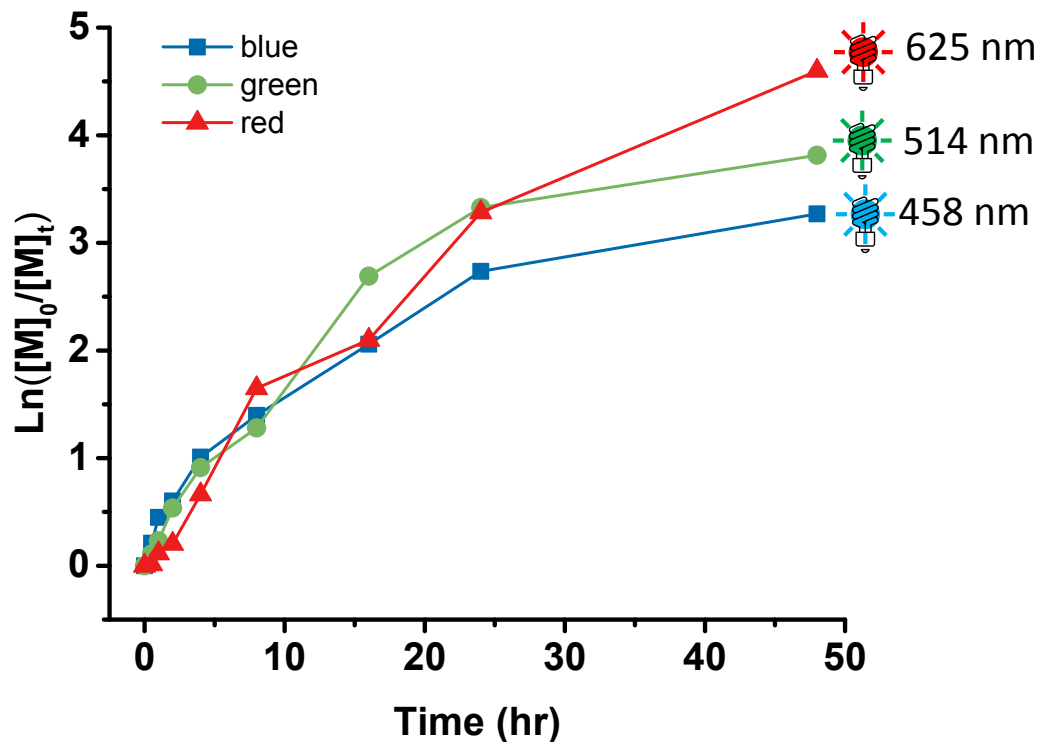


**Figure 10.** A) Illustration of PET-RAFT step-growth mechanism and B) semi-logarithmic plot. Adapted with permission from reference.<sup>49</sup> Copyright 2022, with permission from Royal Society of Chemistry.

## 7 Graft copolymers from RAFT step-growth polymers

Graft copolymers have attracted interest in various fields in academia, owing to unique solution, bulk, and colloidal properties, where applications can be found in drug delivery to plastics.<sup>77-79</sup> However, preparing such molecular architecture can be challenging, as it requires construction of the main chain backbone and polymeric side chains (also known as grafts) on a single macromolecule. Three prevailing synthetic approaches have been actively pursued: (a) polymerizing the mainchain backbone with macromonomers (Graft-through), (b) polymerizing the grafts from the mainchain backbone (Graft from), and (c) attaching end-group functional pre-grafts to the mainchain backbone (Graft-to). In all three approaches, post-polymerization modification or two orthogonal polymerization techniques are employed.<sup>80</sup>

Owing to the retention of the CTA functionality, the RAFT step-growth polymers can be used to directly graft from the backbone via RAFT chain-growth polymerization without any additional step in between, thereby greatly simplifying the preparation of such complex polymers. One characteristic feature of successful synthesis of the graft copolymers is the clear shift in the molecular weight distribution via SEC analysis. Additional evidence can be obtained from absolute  $M_n$  (determined by light scattering) being consistent with the theoretical molecular weight; the latter can be calculated from monomer conversion of the monomers for the graft and absolute  $M_n$  of the precursor mainchain backbone. It is important to note that, appropriate polymerization conditions have to be carefully chosen to minimize intermolecular brush-brush coupling from radical termination events between graft chain ends.

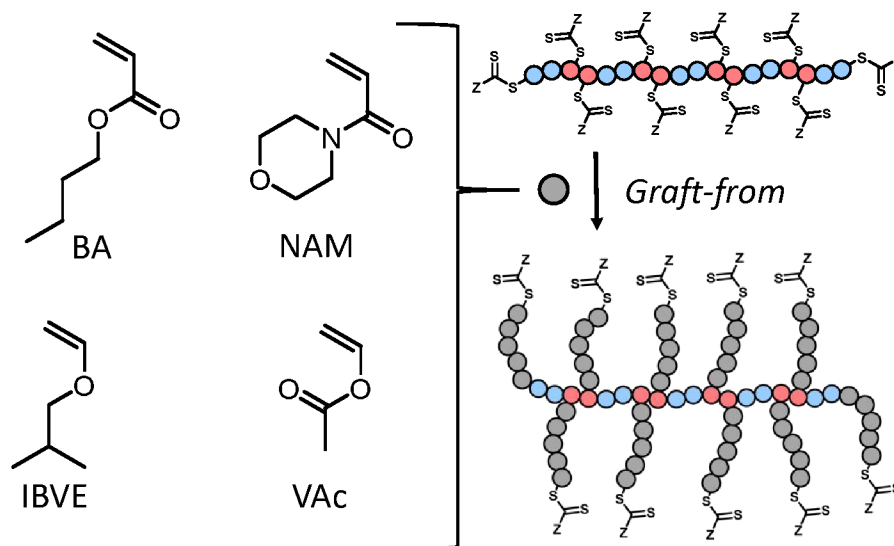


**Chart 2.** Reported monomers for graft copolymerization with RAFT step-growth polymers: Butyl Acrylate (BA), *N*-Acryloyl Morpholine (NAM), Vinyl Acetate (VAc) and IsoButyl Vinyl Ether (IBVE).

### 7.1 Grafting from maleimidic RAFT step-growth backbone

Butyl acrylate (BA) graft copolymers have been reported by grafting from  $P(M_{2Si}\text{-}alt\text{-}CTA_{2A})$  and  $P(M_{2A}\text{-}alt\text{-}CTA_{2SS})$  backbones,<sup>16, 49</sup> whilst *N*-acryloyl morpholine (NAM) graft copolymer has been reported by grafting from  $P(M_{2A}\text{-}alt\text{-}CTA_{2A})$  backbone.<sup>52</sup> In all cases, successful shift in the molecular weight

distribution via SEC was observed; additionally, P(M<sub>2A</sub>-*alt*-CTA<sub>2A</sub>)-*g*-PNAM revealed the expected increase in absolute  $M_n$  ( $M_{n,LS} = 205k$ ,  $M_{n,th} = 213k$ ).<sup>52</sup>

Furthermore, taking advantage of the scalability of the RAFT step-growth backbone (e.g., using commercially available bismaleimides), Boeck et al. achieved multigram preparation of Poly(*N*-acryloyl morpholine) (PNAM) graft copolymer (15 grams, 93 % recovery).<sup>52</sup> It is worth noting that, PNAM has attracted great interest for biomedical applications as potential alternative to polyethylene glycol (PEG).<sup>81</sup> Following end-group removal to allow aqueous solubility, dynamic light scattering (DLS) analysis revealed this PNAM graft copolymer had a Z-average hydrodynamic diameter of 22 nm with polydispersity index (PDI) of 0.210. A single macromolecule of this size can be used for applications in tumor targeted drug delivery,<sup>82, 83</sup> highlighting the potential utility of RAFT step-growth polymers.

### 7.2 Grafting from acrylic RAFT step-growth backbone

BA graft copolymers has also been reported by grafting from (P(M<sub>2E</sub>-*alt*-CTA<sub>2A</sub>), P(M<sub>2E</sub>-*alt*-CTA<sub>2SS</sub>) and P(M<sub>2G</sub>-*alt*-CTA<sub>2A</sub>) backbones.<sup>21</sup> In all cases, successful shift in the molecular weight distribution via SEC was observed. Additionally, the related Mark-Houwink plot revealed a decrease in the  $\alpha$  value, suggesting more compact behavior of such graft copolymers in solution (**Figure 6F**).

### 7.3 Grafting from vinyl ether RAFT step-growth backbone

The step-growth backbone formed between vinyl ether and xanthate based CTA, P(MCTA<sub>B</sub>), presents a unique opportunity to graft other monomers via cationic or radical RAFT chain-growth polymerization. For example, cationic RAFT polymerization was carried out with isobutyl vinyl ether (IBVE) catalyzed by ZnCl<sub>2</sub>, whilst radical RAFT polymerization was carried out with vinyl acetate (VAc) with thermal initiation by AIBN. Clear shift in SEC traces was observed in both cases (**Figure 11**).<sup>65</sup>

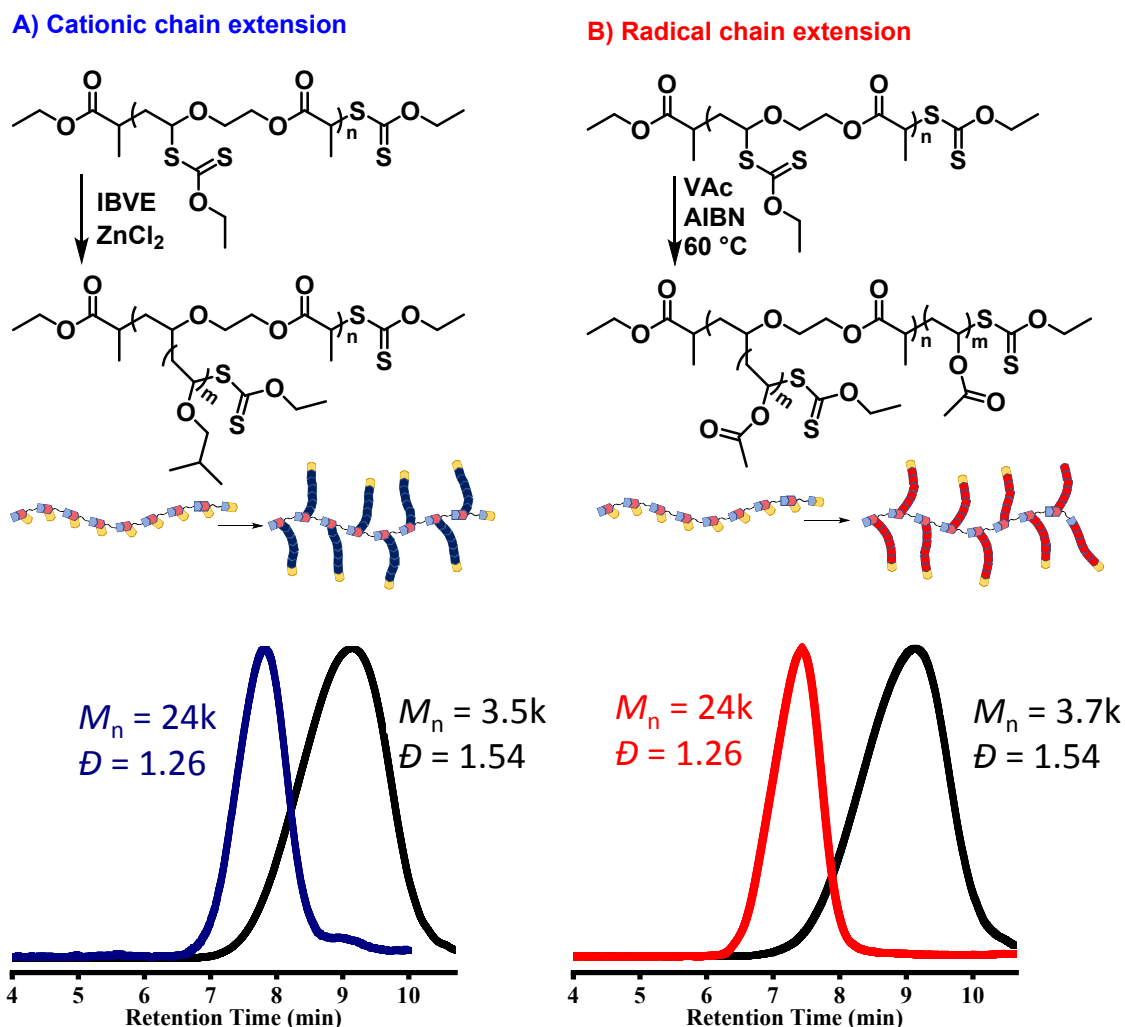


**Figure 11.** SEC traces of IBVE (A) and VAc (B) graft copolymer and its precursor backbone. Adapted with permission from ref. <sup>65</sup> Copyright 2022, with permission from American Chemical Society.

#### 7.4 Grafting from allylic RAFT step-growth backbone

RAFT step-growth backbones based on allylic monomers, such as  $P(M_{2I}\text{-alt-CTA}_{2B})$ ,  $P(M_{2K}\text{-alt-CTA}_{2B})$ ,  $P(M_{2L}\text{-alt-CTA}_{2B})$  and  $P(M_{2M}\text{-alt-CTA}_{2B})$  (**Figure 7**), have been successfully grafted with vinyl acetate (VAc). Additionally, fluorescent acrylate was grafted onto a Living Polymer Network (LPN) (**Figure 12A**, via allylic based RAFT step-growth) using a digitally masked photolithography with a commercial 3D printer (**Figure 12B**). The LPN was prepared from trifunctional vinyl monomer and CTA<sub>2B</sub>, and a type I photo-initiator, 2,4,6-trimethylbenzoyldiphenyl phosphine oxide (TPO), to accelerate the photo crosslinking process.<sup>56</sup>

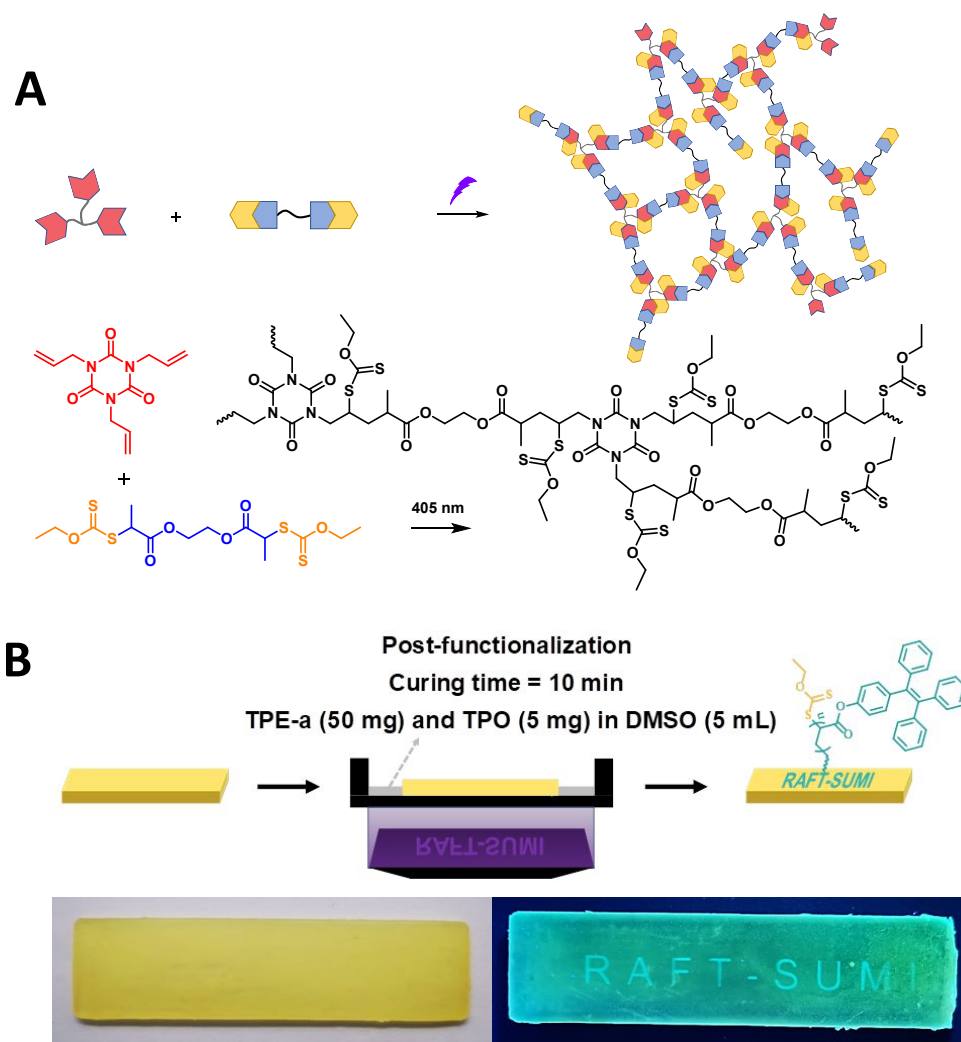


**Figure 12.** Postfunctionalization process with fluorescent acrylate monomer. The film after surface modification under natural light and the film after surface modification under UV light ( $\lambda_{\text{max}} = 365 \text{ nm}$ ). Adapted with permission from ref.<sup>56</sup> Copyright 2023, with permission from Wiley.

### 7.5 Degradable graft copolymers

A unique feature of the brush polymers via grafting from RAFT step-growth backbone is the ability to incorporate specific functionality into the polymer backbone, specifically, via the installation of these functionalities into the initial bifunctional reagents ( $\text{CTA}_2$  or  $\text{M}_2$ ). Moreover,  $\text{A}_2 + \text{B}_2$  RAFT step-growth allows the modular placement of functionality via either bifunctional monomer unit ( $\text{M}_2$ ) or bifunctional CTA unit ( $\text{CTA}_2$ ) or even both.

Placement of functionality along the  $\text{M}_2$  unit of the graft copolymer backbone was demonstrated in the original report, with bismaleimide based RAFT step-growth backbone.<sup>16</sup> PBA graft copolymer,  $\text{P}(\text{M}_{2\text{Si}}\text{-alt-CTA}_{2\text{A}})\text{-g-PBA}$ , which bears cleavable silyl ether within each repeat unit along the length of the backbone, demonstrated rapid stimuli triggered degradation into well-defined linear polymers ( $M_n = 9.0\text{k}$ ,  $D = 1.08$ )

(**Figure 13A**); this value was consistent with the expected molecular weight for two PBA grafts ( $M_{n,th} = 4.9k$  per grafts) upon cleavage of the backbone.

Furthermore, functionality placed in the CTA<sub>2</sub> unit of the graft copolymer backbone was demonstrated in a later report, with the diacrylate based RAFT step-growth backbone.<sup>21</sup> PBA graft copolymer, P(M<sub>2E</sub>-*alt*-CTA<sub>2SS</sub>)-*g*-PBA, which bears cleavable disulfide within each repeat unit along the length of the backbone, also demonstrated stimuli triggered degradation into well-defined linear polymers ( $M_n = 11k$ ,  $\mathcal{D} = 1.12$ ). Again, this value was close to the expected molecular weight of 2 polymeric side chains ( $M_{n,th} = 4.0k$  per side chain) (**Figure 13B**). More recently, UV light was used to partially degrade disulfide functionality in the CTA<sub>2</sub> of PBA graft copolymer prepared from P(M<sub>2A</sub>-*alt*-CTA<sub>2SS</sub>) backbone.<sup>49</sup>

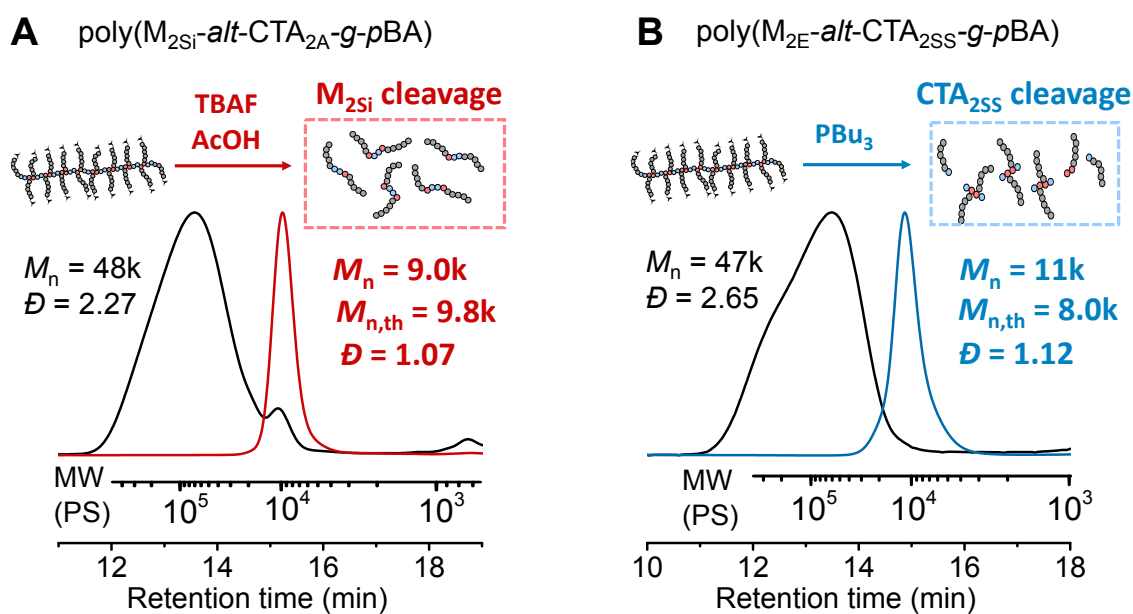


**Figure 13.** Preparation of graft copolymers with degradable backbone. Cleavable unit introduced through the M<sub>2</sub> unit (A) and CTA<sub>2</sub> unit (B). Adapted with permission from ref.<sup>16,21</sup> Copyright 2021 and 2022, with permission from American Chemical Society.

## 8 Classification of RAFT step-growth and RAFT-SUMI

In this section, we present classification of RAFT step-growth and RAFT-SUMI based on the driving force. Particularly, we suggest to use the term ‘ $C_{tr}/C_{-tr}$ ’ as a parameter that governs the efficiency of a given monomer and CTA to undergo RAFT-SUMI process.

### 8.1 $C_{tr}/C_{-tr}$ defining the efficiency of RAFT-SUMI process

In the literature, kinetic modeling of RAFT-SUMI process through numerical analysis has been well-established by Moad et al.<sup>23, 84</sup> Their works led to insightful validation of the importance of specific rate constants in the RAFT-SUMI mechanism. One of the major parameters that has been given high attention is the chain transfer constant ( $C_{tr}$ ), which by itself describes the likelihood of forward chain transfer ( $k_{tr}$ ) over homopropagation ( $k_p$ ). Moad et al. emphasized that  $C_{tr}$  should be sufficiently high to permit one monomer to be inserted per activation cycle ( $k_p \ll k_{tr}$ ).<sup>33</sup> Additionally, they highlighted that the efficiency of SUMI process benefits from rapid  $R\bullet$  addition to the monomer ( $k_i$ ).<sup>33</sup> On the other hand, Xu et al. have experimentally validated the importance of the equilibrium between forward and reverse chain transfer ( $k_{tr}/k_{-tr}$ ) in their investigations, specifically comparing SUMI process of *N*-substituted maleimides with CTA bearing primary and secondary benzyl radical fragmentation.<sup>38, 85</sup> Moreover, Xu et al. focused on RAFT-SUMI process using low  $k_p$  monomers to minimize homopropagation. Furthermore, iterative SUMI was achieved by employing specific pairing of the monomer to fragmentation of the CTA to promote high  $k_i$ .<sup>36</sup>

The question naturally arises: “for a given CTA and monomer pair, how do the all the rate constants (that have been identified to play an important role) orchestrate the efficiency of the SUMI process?” Surprisingly, to date, there has been no simple formula that describes the efficiency of SUMI process. In answering this question, we first define the likelihood of SUMI occurring over homopropagation as a measure of efficiency of the SUMI process. This can be simply defined by a ratio of the key steps that we define for each process, specifically the bimolecular reaction of monomer between  $R\bullet$  species and  $M\bullet$  species:

$$L_{SUMI} = \frac{k_i[M][R\bullet]}{k_p[M][M\bullet]} \quad \text{Eq 14}$$

Herein, we use  $L_{SUMI}$  to define the likelihood of occurrence of SUMI over homopropagation.

Here, we make a key assumption that the chain transfer process of the CTA outweighs all other processes such that the equilibrium between forward and reverse chain transfer is instantaneously reached:

$$k_{tr}[M\bullet][RZ] = k_{-tr}[R\bullet][MZ] \quad \text{Eq 15}$$

Where  $MZ$  represents the fragmentation product between CTA with  $M\bullet$ , and  $RZ$  represents the fragmentation product between CTA with  $R\bullet$  (**Scheme 5**). By definition,  $k_{tr}/k_{-tr}$  describes the equilibrium constant of chain transfer,  $K_{eq}$ :

$$K_{eq} = \frac{k_{tr}}{k_{-tr}} = \frac{[MZ][R\bullet]}{[RZ][M\bullet]} \quad \text{Eq 16}$$

Please note that  $K_{eq}$  is a thermodynamic relationship primarily driven by the relative stability difference between in  $R\bullet$  and the monomer adduct radical species ( $M\bullet$  in **Scheme 5**), which can be intuitively described by the effect of the substituents on relative radical stability.

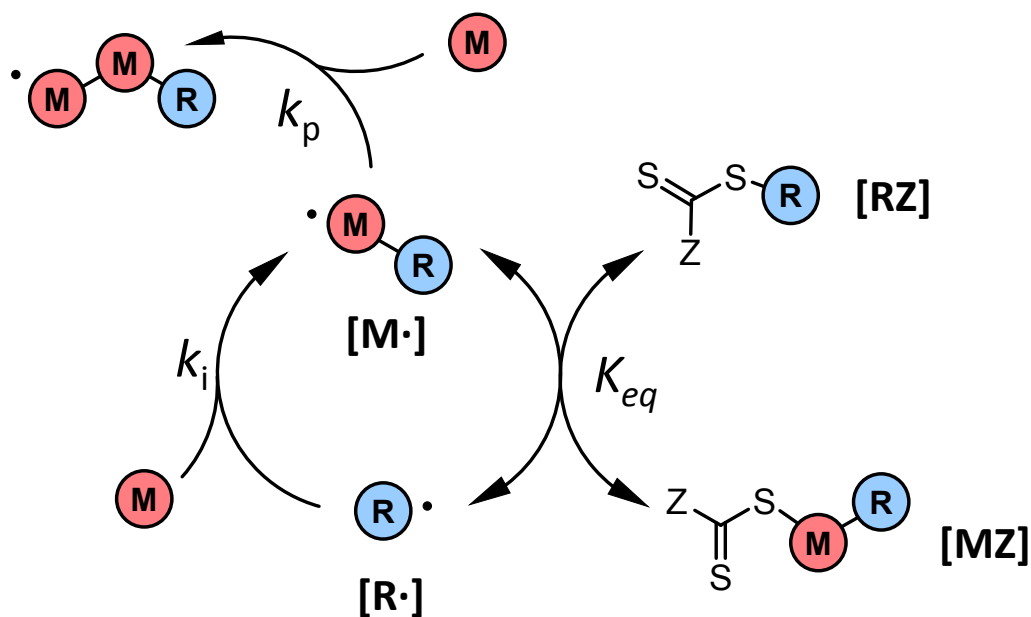
By rearrangement of equation 16,  $[R\cdot]/[M\cdot]$  can be expressed as  $K_{eq}[RZ]/[MZ]$ , which is then substituted into the equation 14 to result in equation 17:

$$L_{SUMI} = \frac{k_i}{k_p} K_{eq} \frac{[RZ]}{[MZ]} \quad \text{Eq 17}$$

More importantly, this equation unifies all rate constants that were identified to play an important role, as a single constant to define efficiency of SUMI to occur for a given monomer and CTA pairing. It is noteworthy that this unification of the three parameters:  $k_i$ ,  $k_p$  and  $K_{eq}$  (or  $k_{tr}/k_{-tr}$ ) can be simply described from the ratio of the forward and reverse chain transfer constants ( $C_{tr}/C_{-tr}$ , where  $C_{tr} = k_{tr}/k_p$  and  $C_{-tr} = k_{-tr}/k_i$ ):

$$\frac{C_{tr}}{C_{-tr}} = K_{eq} \frac{k_i}{k_p} \quad \text{Eq 18}$$

It is worth noting that the premise of equation 17 assumes that chain transfer equilibrium is rapidly reached and therefore only applicable with suitable Z-group for a given monomer class (as it depends on C=S reactivity). It is important to note that neither radical termination nor retardation by the formation of the chain transfer intermediate adduct is considered. In addition, the likelihood of SUMI over homopropagation defined in the formula above ( $L_{SUMI}$ ) depends on the concentration of the initial CTA ( $[RZ]$ ) and monomer adduct / macro-CTA ( $[MZ]$ ), whilst being independent of the monomer concentration. It is also worth noting that the stoichiometry of the monomer to CTA will affect  $[RZ]/[MZ]$  ratio as the limiting reagent is fully consumed. For example, if the monomer was the limiting reagent,  $L_{SUMI}$  is higher at high monomer conversion, than the case if CTA was the limiting reagent. This is because in the former case, the presence of unreacted CTA will result in a relatively higher ratio of  $[RZ]/[MZ]$ ; by contrast, when CTA is the limiting reagent, there will be presence of unreacted monomer after the full consumption of the initial CTA (RZ) and result in a low  $L_{SUMI}$  value.



**Scheme 5.** Illustration of relevant parameters in determining the likelihood of RAFT-SUMI over homopropagation ( $L_{SUMI}$ ).

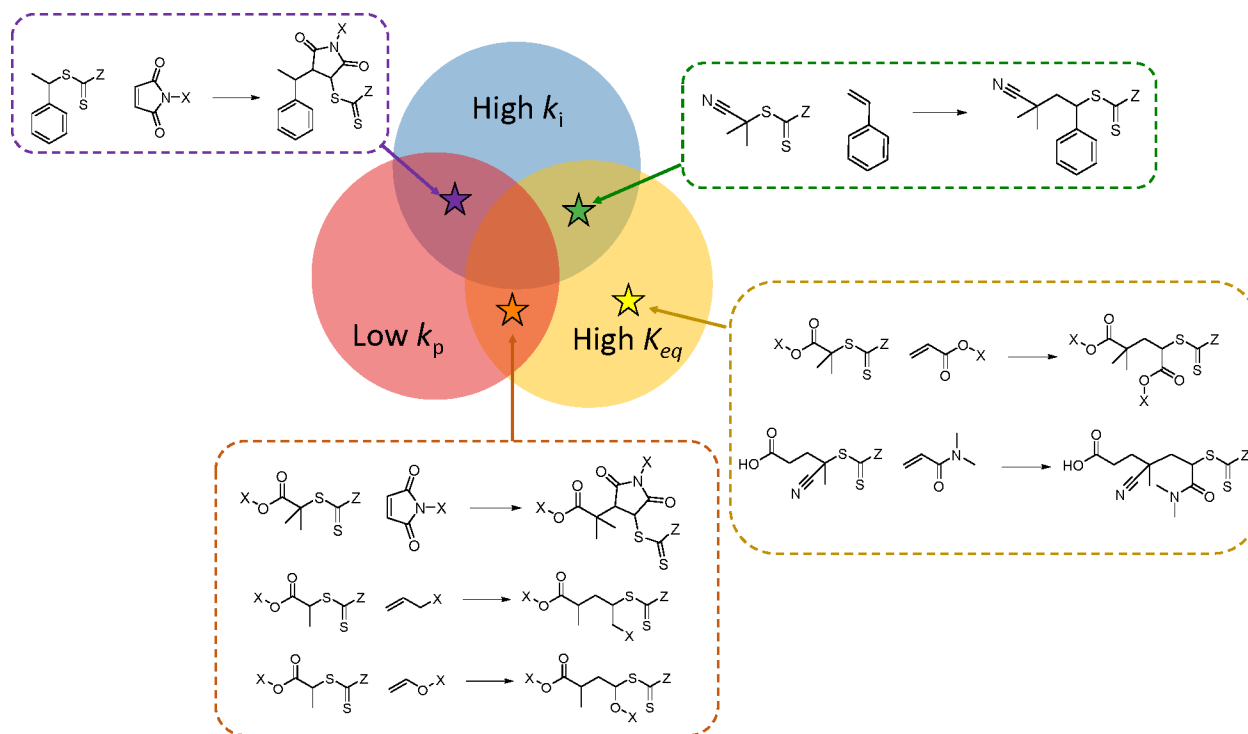
## 8.2 Classification of RAFT step-growth and SUMI based on $k_i$ , $k_p$ and $K_{eq}$

It is important to note that, according to equation 17, the efficiency of SUMI process falls with increasing formation of monomer-adduct (MZ) and consumption of the initial CTA (RZ). Indeed, for high yielding RAFT-SUMI process,  $C_{tr}/C_{-tr}$  would have to be sufficiently high, such that the odds of SUMI occurring over homopropagation is still high even at high CTA conversions. Assuming all reported RAFT step-growth and RAFT-SUMI bears high  $C_{tr}/C_{-tr}$ , we can intuitively categorize most of the reported examples into three overlapping classes (**Scheme 6**) based on three parameters  $k_i$ ,  $k_p$  and  $K_{eq}$  that we believe gives rise to high  $C_{tr}/C_{-tr}$  (equation 18).

For example, reported RAFT-SUMI of acrylate<sup>21</sup> or acrylamide-based<sup>23</sup> monomers using CTA bearing tertiary carboxyalkyl or cyanoalkyl stabilized fragmentation, respectively, can be classified under the high  $K_{eq}$  category (higher radical stability of  $R\cdot$  species relative to  $M\cdot$  promoting high  $K_{eq}$ ). Other reported examples can be categorized as combinations of at least two classes. Examples of RAFT step-growth and RAFT-SUMI with low  $k_p$  monomers have been demonstrated with either high  $k_i$  or high  $K_{eq}$ . For example, RAFT step-growth of maleimides with CTA bearing tertiary carboxyalkyl fragmentation,<sup>16, 52</sup> and vinyl ethers/allyl monomers with CTA bearing secondary carboxyalkyl fragmentation,<sup>55, 56</sup> would fall under the overlapping class of low  $k_p$  and high  $K_{eq}$  (**Scheme 6**).

On the other hand, Xu et al. demonstrated RAFT-SUMI process of CTA bearing secondary benzyl radical fragmentation with *N*-substituted maleimides, which is driven largely by relatively high  $k_i$  and low  $k_p$ <sup>38</sup> (**Scheme 6**). To achieve low  $k_p$ , one could employ beta-alpha substituted monomers;<sup>36</sup> furthermore, employing monomers of different electronic properties (e.g., indene vs. maleimide) could promote higher  $k_i$  to  $k_p$ .<sup>85</sup> All these examples would fall under the overlapping class of high  $k_i$  and low  $k_p$ .

Lastly, the example of RAFT-SUMI of styrene with CTA bearing tertiary cyanoalkyl fragmentation mentioned above (**Figure 1**), can be categorized as an overlapping class of high  $K_{eq}$  (owing to more favorable fragmentation) and high  $k_i$  (considering the monomer addition to  $R\cdot$  is more rapid than the homopropagation) (**Scheme 6**).

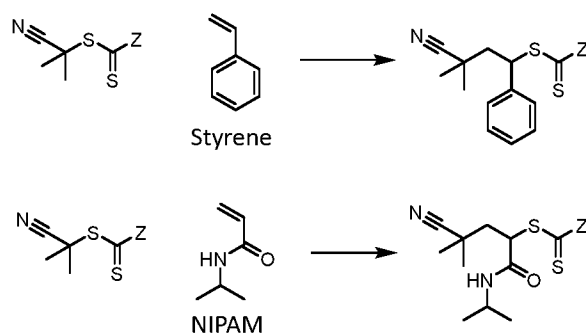


**Scheme 6.** Qualitative classification of RAFT-SUMI and RAFT step-growth systems based on the driving force.

### 8.3 Example of high $C_{tr}/C_{-tr}$ RAFT-SUMI with reported kinetic rate constants

We emphasize that relating SUMI efficiency with  $C_{tr}/C_{-tr}$  (equation 18) is mostly practical for qualitative discussions, as determining value of  $C_{tr}/C_{-tr}$  for a given monomer and CTA pair can be difficult. Generally, rate constants can vary with methods used to determine the values and are subjective on experimental conditions. Additionally, it is worth noting that the  $k_p$  is chain length dependent for many classes of monomers, where the first propagation step ( $k_p(1)$ ) is often faster than subsequent propagation steps ( $k_p(>1)$ ).<sup>23</sup> When quantitatively assessing the  $C_{tr}/C_{-tr}$  value,  $k_p(1)$  should be considered, especially for classes of monomers that are not radically homopolymerizable where  $k_p(>1)$  is negligible.<sup>36</sup>

Moad et al. reported a comparison of SUMI process of NIPAM and styrene with CTA bearing tertiary substituted cyano-stabilized fragmentation (**Table 3, Figure 14**).<sup>23</sup> In both cases, relatively high  $K_{eq}$  values are determined from the ratio of the reported  $k_{tr}$  and  $k_{-tr}$ , which contribute to promoting high  $C_{tr}/C_{-tr}$  values. However, the  $C_{tr}/C_{-tr}$  value is higher for styrene than for NIPAM by an order of magnitude, as the value for  $k_p$  is significantly higher for NIPAM than for styrene whilst  $k_i$  is noticeably higher for styrene than for NIPAM. The latter explains faster RAFT-SUMI kinetics for styrene (**Figure 14**), when considering monomer addition to  $R\cdot$  to be the rate determining step. Interestingly, NIPAM with  $C_{tr}/C_{-tr}$  value of 125 was reported with isolated SUMI-CTA adduct yield of  $\sim 80\%$  (**Figure 14**);<sup>23</sup> by contrast, styrene, with a  $C_{tr}/C_{-tr}$  value of 1092, reveals more quantitative SUMI-CTA adduct yield, which was consistent with similar report by McLeary (using a more active Z-group, **Figure 1**).<sup>27</sup> Thus based on these reports, we suggest that  $C_{tr}/C_{-tr}$  would be required to be higher than  $\sim 10^2$  to allow efficient RAFT-SUMI at high CTA consumption.

**Table 3.** Kinetic parameters of RAFT-SUMI with styrene vs NIPAM

Rate constant / units <sup>a</sup>	Styrene	NIPAM
$k_i / \text{M}^{-1}\text{s}^{-1}$	$5.2 \times 10^3$	$8.0 \times 10^2$
$k_p / \text{M}^{-1}\text{s}^{-1}$	$8.4 \times 10^2$	$1.60 \times 10^3$
$k_{tr} / \text{M}^{-1}\text{s}^{-1}$	$1.5 \times 10^6$	$2.0 \times 10^6$
$k_{-tr} / \text{M}^{-1}\text{s}^{-1}$	$8.5 \times 10^3$	$8.0 \times 10^3$
$K_{eq}^b$	176	250
$C_{tr}/C_{-tr}^c$	1092	125

<sup>a</sup> Rate constants obtained from reference.<sup>23</sup> The  $k_p$  tabulated above is specific value for the first monomer propagation step (to form DP of 2).

<sup>b</sup> Equilibrium constant obtained from  $k_{tr}/k_{-tr}$

<sup>c</sup> Calculated from Equation 18

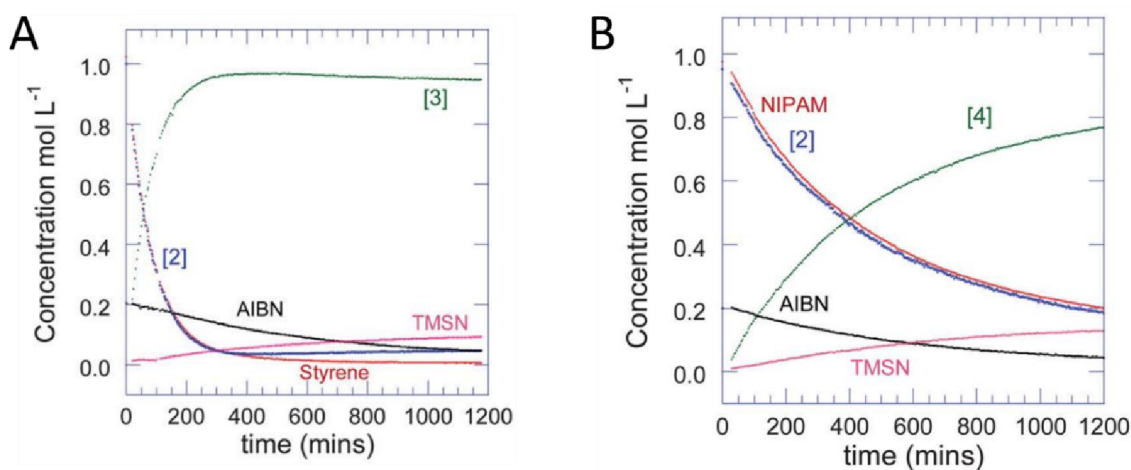


**Figure 14.** RAFT-SUMI kinetics of A) Styrene and B) NIPAM using trithiocarbonate based CTA bearing tertiary cyano-stabilized fragmentation. Figure adapted from ref.<sup>23</sup> Copyright 2012, with permission from Royal Society of Chemistry.

## 9 Conclusions

At the time of this review, RAFT step-growth polymerization has been successfully demonstrated with several monomer families, including maleimides, acrylates, vinyl ethers and allylics. In theory, an appropriate pair of monomer and CTA that generates quantitative SUMI-CTA adduct yields with monomer conversion, can be designed into bifunctional reagents ( $AB$ , or  $A_2 + B_2$ ) to allow successful RAFT step-growth polymerization. Given the prior literature reports in RAFT initialization and SUMI process, we predict an expansion of the monomer scope for RAFT step-growth polymerization. Furthermore, we anticipate further development and identification of new monomer and CTA pairs for efficient RAFT-SUMI process, by judiciously selecting the relevant parameters ( $k_i$ ,  $k_p$  and  $K_{eq}$ ) to achieve high efficiency ( $C_{tr}/C_{-tr}$ ). It is important to note that selectivity may arise from activation-deactivation process (iniferter, redox or PET) in some cases where the chain transfer process is limiting.

From a practical perspective, RAFT step-growth polymerization synergistically combines features of traditional RAFT polymerization (high functional group tolerance, user-friendly nature) and traditional step-growth (versatility in backbone design) and offers new opportunities to prepare complex architectures with synthetic ease. We anticipate the broad application of the linear and graft copolymers from RAFT step-growth polymerization in materials science, for example, drug-delivery, by taking advantage of the versatility of the backbone to introduce biodegradability.

Lastly, we would like to emphasize the characterization of step-growth polymerization by following  $M_n$ ,  $M_w$  and  $M_z$  rather than traditional characterization with  $M_n$  and  $D$  only. This practice allows better comparison of experimental data with Flory's classical model of the expected linear molecular weight evolution to evaluate step-growth polymerizations.

## AUTHOR INFORMATION

### Corresponding Author

\* Joji Tanaka-Department of Chemistry, University of North Carolina, Chapel Hill, NC 27599, USA. Email: [joji@email.unc.edu](mailto:joji@email.unc.edu)

\* Wei You - Department of Chemistry, University of North Carolina, Chapel Hill, NC 27599, USA. Email: [wyou@unc.edu](mailto:wyou@unc.edu)

## ACKNOWLEDGMENT

This work was financially supported by the National Science Foundation (NSF) under Award CHE-2108670.

## References

1. V. P. Beyer, J. Kim and C. R. Becer, *Polymer Chemistry*, 2020, **11**, 1271-1291.
2. N. Corrigan, J. Yeow, P. Judzewitsch, J. Xu and C. Boyer, *Angew. Chem. Int. Ed.*, 2019, **58**, 5170-5189.
3. J. Yeow, R. Chapman, A. J. Gormley and C. Boyer, *Chem. Soc. Rev.*, 2018, **47**, 4357-4387.
4. S. Oliver, L. Zhao, A. J. Gormley, R. Chapman and C. Boyer, *Macromolecules*, 2019, **52**, 3-23.
5. C. H. Chan, J.-T. Chen, W. S. Farrell, C. M. Fellows, D. J. Keddie, C. K. Luscombe, J. B. Matson, J. Merna, G. Moad, G. T. Russell, P. Théato, P. D. Topham and L. Sosa Vargas, *Polym. Chem.*, 2022, **13**, 2262-2270.
6. R. B. Grubbs and R. H. Grubbs, *Macromolecules*, 2017, **50**, 6979-6997.
7. L. Billiet, D. Fournier and F. Du Prez, *Polymer*, 2009, **50**, 3877-3886.
8. M. Destarac, *Polym. Chem.*, 2018, **9**, 4947-4967.
9. N. Corrigan, K. Jung, G. Moad, C. J. Hawker, K. Matyjaszewski and C. Boyer, *Progress in Polymer Science*, 2020, **111**, 101311.
10. J. Chiefari, Y. K. Chong, F. Ercole, J. Krstina, J. Jeffery, T. P. T. Le, R. T. A. Mayadunne, G. F. Meijs, C. L. Moad, G. Moad, E. Rizzardo and S. H. Thang, *Macromolecules*, 1998, **31**, 5559-5562.
11. J. Chiefari, R. T. A. Mayadunne, C. L. Moad, G. Moad, E. Rizzardo, A. Postma and S. H. Thang, *Macromolecules*, 2003, **36**, 2273-2283.
12. Y. K. Chong, J. Krstina, T. P. T. Le, G. Moad, A. Postma, E. Rizzardo and S. H. Thang, *Macromolecules*, 2003, **36**, 2256-2272.
13. S. Perrier, *Macromolecules*, 2017, **50**, 7433-7447.
14. R. Wei, T. Tiso, J. Bertling, K. O'Connor, L. M. Blank and U. T. Bornscheuer, *Nature Catalysis*, 2020, **3**, 867-871.
15. C. Boyer, M. Kamigaito, K. Satoh and G. Moad, *Prog. Polym. Sci.*, 2023, **138**, 101648.
16. J. Tanaka, N. E. Archer, M. J. Grant and W. You, *J. Am. Chem. Soc.*, 2021, **143**, 15918-15923.
17. N. B. Cramer, S. K. Reddy, A. K. O'Brien and C. N. Bowman, *Macromolecules*, 2003, **36**, 7964-7969.
18. K. Satoh, M. Mizutani and M. Kamigaito, *Chem. Commun.*, 2007, DOI: 10.1039/B616598B, 1260-1262.
19. M. Mizutani, K. Satoh and M. Kamigaito, *Macromolecules*, 2009, **42**, 472-480.
20. M. Kamigaito, *Polym. J.*, 2022, **54**, 1391-1405.
21. N. E. Archer, P. T. Boeck, Y. Ajirniar, J. Tanaka and W. You, *ACS Macro Letters*, 2022, **11**, 1079-1084.
22. J. Xu, *Macromolecules*, 2019, **52**, 9068-9093.
23. S. Houshyar, D. J. Keddie, G. Moad, R. J. Mulder, S. Saubern and J. Tsanaktsidis, *Polymer Chemistry*, 2012, **3**, 1879-1889.
24. P. Delduc, C. Tailhan and S. Z. Zard, *Journal of the Chemical Society, Chemical Communications*, 1988, 308-310.
25. B. Quiclet-Sire and S. Z. Zard, *Pure Appl. Chem.*, 2010, **83**, 519-551.
26. S. Z. Zard, *Macromolecules*, 2020, **53**, 8144-8159.
27. J. B. McLeary, F. M. Calitz, J. M. McKenzie, M. P. Tonge, R. D. Sanderson and B. Klumperman, *Macromolecules*, 2004, **37**, 2383-2394.
28. M. Chen, K. P. Ghiggino, A. W. H. Mau, E. Rizzardo, W. H. F. Sasse, S. H. Thang and G. J. Wilson, *Macromolecules*, 2004, **37**, 5479-5481.
29. J. B. McLeary, J. M. McKenzie, M. P. Tonge, R. D. Sanderson and B. Klumperman, *Chem. Commun.*, 2004, DOI: 10.1039/B404857A, 1950-1951.

30. G. Pound, J. B. McLeary, J. M. McKenzie, R. F. M. Lange and B. Klumperman, *Macromolecules*, 2006, **39**, 7796-7797.
31. J. B. McLeary, F. M. Calitz, J. M. McKenzie, M. P. Tonge, R. D. Sanderson and B. Klumperman, *Macromolecules*, 2005, **38**, 3151-3161.
32. M. Chen, M. Häussler, G. Moad and E. Rizzardo, *Organic & Biomolecular Chemistry*, 2011, **9**, 6111-6119.
33. J. J. Haven, M. Hendriks, T. Junkers, P. J. Leenaers, T. Tsompanoglou, C. Boyer, J. Xu, A. Postma and G. Moad, in *Reversible Deactivation Radical Polymerization: Mechanisms and Synthetic Methodologies*, American Chemical Society, 2018, vol. 1284, ch. 4, pp. 77-103.
34. Y. Zhou, Z. Zhang, C. M. Reese, D. L. Patton, J. Xu, C. Boyer, A. Postma and G. Moad, *Macromol. Rapid Commun.*, 2020, **41**, 1900478.
35. A. Aerts, R. W. Lewis, Y. Zhou, N. Malic, G. Moad and A. Postma, *Macromol Rapid Commun*, 2018, **39**, e1800240.
36. R. Liu, L. Zhang, Z. Huang and J. Xu, *Polym. Chem.*, 2020, **11**, 4557-4567.
37. S. Lin, L. Zhang, Z. Huang, P. V. Kumar and J. Xu, *Macromolecules*, 2019, **52**, 7157-7166.
38. Z. Huang, N. Corrigan, S. Lin, C. Boyer and J. Xu, *Journal of Polymer Science Part A: Polymer Chemistry*, 2019, **57**, 1947-1955.
39. C. Fu, Z. Huang, C. J. Hawker, G. Moad, J. Xu and C. Boyer, *Polymer Chemistry*, 2017, **8**, 4637-4643.
40. J. Xu, C. Fu, S. Shanmugam, C. J. Hawker, G. Moad and C. Boyer, *Angewandte Chemie International Edition*, 2017, **56**, 8376-8383.
41. J. J. Haven, J. Vandenbergh, R. Kurita, J. Gruber and T. Junkers, *Polym. Chem.*, 2015, **6**, 5752-5765.
42. J. Vandenbergh, G. Reekmans, P. Adriaensens and T. Junkers, *Chem. Commun.*, 2013, **49**, 10358-10360.
43. D. J. Keddie, *Chemical Society Reviews*, 2014, **43**, 496-505.
44. G. Odian, in *Principles of Polymerization*, 2004, DOI: <https://doi.org/10.1002/047147875X.ch2>, pp. 39-197.
45. M. Gavrilov and M. J. Monteiro, *Eur. Polym. J.*, 2015, **65**, 191-196.
46. D. T. Gentekos, R. J. Sifri and B. P. Fors, *Nature Reviews Materials*, 2019, **4**, 761-774.
47. P. J. Flory, *J. Am. Chem. Soc.*, 1936, **58**, 1877-1885.
48. J. Rosselgong and S. P. Armes, *Macromolecules*, 2012, **45**, 2731-2737.
49. S. M. Clouthier, J. Tanaka and W. You, *Polymer Chemistry*, 2022, **13**, 6114-6119.
50. F. W. P. C. Corporation, [http://www.wako-chem.co.jp/kaseihin\\_en/oilazo/AIBN.htm](http://www.wako-chem.co.jp/kaseihin_en/oilazo/AIBN.htm)).
51. G. Moad, *Prog. Polym. Sci.*, 2019, **88**, 130-188.
52. P. Boeck, N. Archer, J. Tanaka and W. You, *Polym. Chem.*, 2022, **13**, 2589-2594.
53. Y. Lu, L. An and Z.-G. Wang, *Macromolecules*, 2013, **46**, 5731-5740.
54. K. G. E. Bradford, L. M. Petit, R. Whitfield, A. Anastasaki, C. Barner-Kowollik and D. Konkolewicz, *J. Am. Chem. Soc.*, 2021, **143**, 17769-17777.
55. Z. Li, J. Li, X. Pan, Z. Zhang and J. Zhu, *ACS Macro Letters*, 2022, **11**, 230-235.
56. Z. Li, J. Li, B. Zhao, X. Pan, X. Pan and J. Zhu, *Chinese Journal of Chemistry*, 2023, **41**, 503-508.
57. J. Phommalyasack-Lovan, Y. Chu, C. Boyer and J. Xu, *Chem. Commun.*, 2018, **54**, 6591-6606.
58. T. Otsu, M. Yoshida and T. Tazaki, *Die Makromolekulare Chemie, Rapid Communications*, 1982, **3**, 133-140.
59. J. F. Quinn, L. Barner, C. Barner-Kowollik, E. Rizzardo and T. P. Davis, *Macromolecules*, 2002, **35**, 7620-7627.
60. C.-Y. Hong, Y.-Z. You, R.-K. Bai, C.-Y. Pan and G. Borjihan, *Journal of Polymer Science Part A: Polymer Chemistry*, 2001, **39**, 3934-3939.

61. J. Xu, S. Shanmugam, N. A. Corrigan and C. Boyer, *ACS Symposium Series*, 2015, **1187**, 247-267.
62. S. Shanmugam, J. Cuthbert, J. Flum, M. Fantin, C. Boyer, T. Kowalewski and K. Matyjaszewski, *Polymer Chemistry*, 2019, **10**, 2477-2483.
63. S. Shanmugam, J. Cuthbert, T. Kowalewski, C. Boyer and K. Matyjaszewski, *Macromolecules*, 2018, **51**, 7776-7784.
64. T. G. McKenzie, Q. Fu, M. Uchiyama, K. Satoh, J. Xu, C. Boyer, M. Kamigaito and G. G. Qiao, *Advanced Science*, 2016, **3**, 1500394.
65. Z. Li, J. Li, X. Pan, Z. Zhang and J. Zhu, *ACS Macro Letters*, 2022, **11**, 230-235.
66. P. N. Kurek, A. J. Kloster, K. A. Weaver, R. Manahan, M. L. Allegranza, N. De Alwis Watuthanthrige, C. Boyer, J. A. Reeves and D. Konkolewicz, *Industrial & Engineering Chemistry Research*, 2018, **57**, 4203-4213.
67. M. L. Allegranza and D. Konkolewicz, *ACS Macro Letters*, 2021, **10**, 433-446.
68. J. Xu, K. Jung, A. Atme, S. Shanmugam and C. Boyer, *J Am Chem Soc*, 2014, **136**, 5508-5519.
69. J. Xu, K. Jung, N. A. Corrigan and C. Boyer, *Chemical Science*, 2014, **5**, 3568-3575.
70. N. Corrigan, J. Xu, C. Boyer and X. Allonas, *ChemPhotoChem*, 2019, **3**, 1193-1199.
71. S. Shanmugam, J. Xu and C. Boyer, *J Am Chem Soc*, 2015, **137**, 9174-9185.
72. J. Yeow and C. Boyer, *Advanced Science*, 2017, **4**, 1700137.
73. J. Xu, S. Shanmugam, H. T. Duong and C. Boyer, *Polym. Chem.*, 2015, **6**, 5615-5624.
74. R. N. Carmean, M. B. Sims, C. A. Figg, P. J. Hurst, J. P. Patterson and B. S. Sumerlin, *ACS Macro Letters*, 2020, **9**, 613-618.
75. C. A. Figg, J. D. Hickman, G. M. Scheutz, S. Shanmugam, R. N. Carmean, B. S. Tucker, C. Boyer and B. S. Sumerlin, *Macromolecules*, 2018, **51**, 1370-1376.
76. Y. Zhou, Z. Zhang, C. M. Reese, D. L. Patton, J. Xu, C. Boyer, A. Postma and G. Moad, *Macromol Rapid Commun*, 2020, **41**, e1900478.
77. G. Xie, M. R. Martinez, M. Olszewski, S. S. Sheiko and K. Matyjaszewski, *Biomacromolecules*, 2019, **20**, 27-54.
78. S. S. Sheiko and A. V. Dobrynin, *Macromolecules*, 2019, **52**, 7531-7546.
79. M. Müllner, *Macromol. Chem. Phys.*, 2016, **217**, 2209-2222.
80. D. C. Lee, R. J. Lamm, A. N. Prossnitz, A. J. Boydston and S. H. Pun, *Advanced Healthcare Materials*, 2019, **8**, 1800861.
81. T. T. Hoang Thi, E. H. Pilkington, D. H. Nguyen, J. S. Lee, K. D. Park and N. P. Truong, *Polymers*, 2020, **12**, 298.
82. H. Cabral, Y. Matsumoto, K. Mizuno, Q. Chen, M. Murakami, M. Kimura, Y. Terada, M. R. Kano, K. Miyazono, M. Uesaka, N. Nishiyama and K. Kataoka, *Nature Nanotechnology*, 2011, **6**, 815.
83. S. Kaga, N. P. Truong, L. Esser, D. Senyschyn, A. Sanyal, R. Sanyal, J. F. Quinn, T. P. Davis, L. M. Kaminskas and M. R. Whittaker, *Biomacromolecules*, 2017, **18**, 3963-3970.
84. C. H. J. Johnson, T. H. Spurling and G. Moad, *Polymers*, 2022, **14**, 5013.
85. Z. Huang, B. B. Noble, N. Corrigan, Y. Chu, K. Satoh, D. S. Thomas, C. J. Hawker, G. Moad, M. Kamigaito, M. L. Coote, C. Boyer and J. Xu, *J. Am. Chem. Soc.*, 2018, **140**, 13392-13406.